Monthly Notices
of the
ROYAL ASTRONOMICAL SOCIETY

MNRAS **434,** 2830–2855 (2013) doi:10.1093/mnras/stt1189
Advance Access publication 2013 August 7

New approaches to probing Minkowski functionals

D. Munshi,[1,2]★ J. Smidt,[3,4] A. Cooray,[4] A. Renzi,[5,6,7] A. Heavens[8] and P. Coles[1,2]

[1]*School of Physics and Astronomy, Cardiff University, Queen's Buildings, 5 The Parade, Cardiff CF24 3AA, UK*
[2]*School of Mathematical and Physical Sciences, University of Sussex, Brighton BN1 9QH, UK*
[3]*Los Alamos National Laboratory, Theoretical Division, PO Box 1663, Mail Stop B283, Los Alamos, NM 87545, USA*
[4]*Department of Physics and Astronomy, University of California, Irvine, CA 92697, USA*
[5]*INFN, Sezione di Padova, Via Marzolo 8, I-35131 Padova, Italy*
[6]*Dipartimento di Fisica e Astronomia 'G. Galilei', Universitá degli Studi di Padova, Via Marzolo 8, I-35131 Padova, Italy*
[7]*SISSA, Via Bonomea 265, Trieste I-34136, Italy*
[8]*Imperial Centre for Inference and Cosmology, Department of Physics, Imperial College, Blackett Laboratory, Prince Consort Road, London SW7 2AZ, UK*

Accepted 2013 June 26. Received 2013 May 31; in original form 2013 April 2

ABSTRACT

We generalize the concept of the ordinary skew-spectrum to probe the effect of non-Gaussianity on the morphology of cosmic microwave background (CMB) maps in several domains: in real space (where they are commonly known as *cumulant-correlators*), and in harmonic and needlet bases. The essential aim is to retain more information than normally contained in these statistics, in order to assist in determining the source of any measured non-Gaussianity, in the same spirit as Munshi & Heavens skew-spectra were used to identify foreground contaminants to the CMB bispectrum in *Planck* data. Using a perturbative series to construct the Minkowski functionals (MFs), we provide a pseudo-$\mathcal{C}_\ell$ based approach in both harmonic and needlet representations to estimate these spectra in the presence of a mask and inhomogeneous noise. Assuming homogeneous noise, we present approximate expressions for error covariance for the purpose of joint estimation of these spectra. We present specific results for four different models of primordial non-Gaussianity *local*, *equilateral*, *orthogonal* and *enfolded* models, as well as non-Gaussianity caused by unsubtracted point sources. Closed form results of next-order corrections to MFs too are obtained in terms of a quadruplet of kurt-spectra. We also use the method of *modal decomposition* of the bispectrum and trispectrum to reconstruct the MFs as an alternative method of reconstruction of morphological properties of CMB maps. Finally, we introduce the odd-parity skew-spectra to probe the odd-parity bispectrum and its impact on the morphology of the CMB sky. Although developed for the CMB, the generic results obtained here can be useful in other areas of cosmology.

Key words: methods: analytical – methods: numerical – methods: statistical – cosmic background radiation – diffuse radiation – large-scale structure of Universe.

1 INTRODUCTION

The study of cosmic microwave background (CMB) radiation provides the cleanest window to probe the very early stages of the Universe's history. This can be used to probe the mechanism that generates seed perturbations, which lead to the structure that we observe in the present-day Universe. Recent observations by *Wilkinson Microwave Anisotropy Probe* (*WMAP*)[1] and *Planck*[2] (Tauber et al. 2010) supports the basic predictions of inflationary scenarios. Recent results from *Planck* favour adiabatic and almost Gaussian seed perturbations. Furthermore, in future the proposed Experimental Probe of Inflationary Cosmology (EPIC) survey, or ESA's *Cosmic Origin Explorer* (*COrE*) or Polarized Radiation Imaging and Spectroscopy Mission (PRISM;[3] The COrE Collaboration 2011), fourth-generation CMB satellite mission concepts, are very important in furthering our knowledge of the Universe. See e.g. Kermish et al. (2012) for the POLARBEAR[4] experiment. The

★E-mail: D.Munshi@sussex.ac.uk
[1] http://map.gsfc.nasa.gov/
[2] http://www.rssd.esa.int/index.php?project=Planck
[3] http://www.prism-mission.org/
[4] http://bolo.berkeley.edu/polarbear/

current generation of ground-based observations, namely the Atacama Cosmology Telescope (ACT; see Niem et al. 2010 for ACTPol)[5] as well as the South Pole Telescope (SPT; see McMahon et al. 2009 for SPTPol)[6] are already providing important clues especially of the CMB *secondary* anisotropy at smaller angular scales, i.e. below a few arcminutes. It is well established now that non-Gaussianity (NG) from simplest inflationary models based on a single slowly rolling scalar field is typically very small (Salopek & Bond 1990, 1991; Falk et al. 1993; Gangui et al. 1994; Acquaviva et al. 2003; Maldacena 2003) (see e.g. Bartolo, Matarrese & Riotto 2006 for a review). However, there are many variants of simple inflationary models which include models with multiple scalar fields (Linde & Mukhanov 1997; Lyth, Ungarelli & Wands 2003), features in the inflationary potential, non-adiabatic fluctuations, non-standard kinetic terms, warm inflation (Gupta, Berera & Heavens 2002; Moss & Xiong 2007), or deviations from Bunch–Davies vacuum that can all lead to much higher level of NG, but these are heavily constrained by Planck limits (Planck Collaboration 2013).

Early observational work on the bispectrum from *COBE* (Komatsu et al. 2002) and Millimetre Anisotropy eXperiment IMaging Survey (MAXIMA; Santos et al. 2003) was followed by much more accurate analysis with *WMAP* (Komatsu et al. 2003; Creminelli et al. 2007a; Spergel et al. 2007) and *Planck* (Planck Collaboration 2013). Much of the interest in primordial NG has focused on a phenomenological '*local* $f_{\rm NL}$' parametrization in terms of the perturbative non-linear coupling in the primordial curvature perturbation (Verde et al. 2000):

$$\Phi(x) = \Phi_L(x) + f_{\rm NL}(\Phi_{\rm L}^2(x) - \langle\Phi_{\rm L}^2(x)\rangle) + g_{\rm NL}\Phi_{\rm L}^3(x) + h_{\rm NL}(\Phi_{\rm L}^4(x) - 3\langle\Phi_{\rm L}^2(x)\rangle^2) + \cdots, \quad (1)$$

where $\Phi_{\rm L}(x)$ denotes the linear Gaussian part of the Bardeen curvature and $f_{\rm NL}$, $g_{\rm NL}$, $h_{\rm NL}$ are the non-linear coupling parameters. A number of models have NG which can be approximated by this form. The leading-order NG therefore is normally at the level of the bispectrum, or in configuration space at the three-point level. Many studies involving primordial NG have used the bispectrum, motivated by the fact that it contains all the information about $f_{\rm NL}$ (Babich 2005 but see Kamionkowski, Smith & Heavens 2011). It has been extensively studied [Creminelli 2003; Komatsu, Spergel & Wandelt 2005 (hereafter KSW); Creminelli et al. 2006; Cabella et al. 2006; Medeiros & Contaldi 2006; Liguori et al. 2007; Yadav, Komatsu & Wandelt 2007; Yadav et al. 2008; Smith, Senatore & Zaldarriaga 2009], with most of these measurements providing convolved estimates of the bispectrum. Optimized three-point estimators were introduced by Heavens (1998), and have been successively developed (Smith, Zahn & Dore 2000; KSW; Creminelli et al. 2006; Smith & Zaldarriaga 2006; Creminelli, Senatore & Zaldarriaga 2007b) to the point where an estimator for $f_{\rm NL}$ which saturates the Cramer–Rao bound exists for partial sky coverage and inhomogeneous noise (Smith et al. 2009). Approximate forms also exist for *equilateral* NG, which may arise in models with non-minimal Lagrangian with higher derivative terms (Chen, Huang & Kachru 2007a; Chen, Easther & Lim 2007b). In these models, the largest signal comes from spherical harmonic modes with $\ell_1 \simeq \ell_2 \simeq \ell_3$, whereas for the local model, the signal is highest when one ℓ is much smaller than the other two – the so-called *squeezed* configuration. The four different models that we consider in this paper are *local*, *equilateral*, *orthogonal* and *enfolded* models of primordial NG (see e.g. Meerburg, van der Schaar & Corasaniti 2007; Komatsu 2010; Yadav & Wandelt 2010 for more detailed discussions about these models; a very short summary is provided in Appendix A).

While the bispectrum or its higher order analogues, multispectra, are more commonly used in studying departure from Gaussianity (Bartolo et al. 2004), alternative statistics such as Minkowski functionals (MFs) too are routinely used for this purpose. MFs describe the morphological features of a fluctuating (random) fields (Mecke, Buchert & Wagner 1994; Schmalzing & Buchert 1997; Schmalzing & Gorski 1998; Winitizki & Kosowsky 1998). The MFs for a Gaussian field are well understood and closed-form expressions exist (Tomita 1986). The MFs have been used to detect NG using projected (2D) fields such as the CMB (Hikage, Komatsu & Matsubara 2006), weak lensing (Matsubara & Jain 2001) and three-dimensional (3D) density fields as mapped by the galaxy surveys e.g. Sloan Digital Sky Survey (Hikage et al. 2002, 2008a; Hikage, Taruya & Suto 2003; Park et al. 2005; Hikage, Komatsu & Matsubara 2006). Several analytical results exist for prescriptions to model non-linear gravity as well as biasing schemes both in the quasi-linear and highly non-linear regimes (Munshi et al. 1995; Hikage et al. 2008a). The MFs have been used also for the study of CMB data e.g. 4-year *COBE* Differential Microwave Radiometer data (Novikov, Schmalzing & Mukhanov 2000), BOOMERanG data (Natoli et al. 2010) as well as for the *WMAP* data (Komatsu et al. 2003; Eriksen et al. 2004; Hikage et al. 2008b; Hikage & Matsubara 2012). The MF-based approach has also been used to study the effect of lensing on the CMB (Schmalzing, Takada & Futamase 2000). Using an MF-based approach on *WMAP* 7-year data Hikage & Matsubara (2012) recently obtained $f_{\rm NL}^{\rm loc} = 20 \pm 42$, $f_{\rm NL}^{\rm equi} = -121 \pm 208$ and $f_{\rm NL}^{\rm orth} = -129 \pm 171$. The recent constraints from *Planck* data release (Planck Collaboration 2013) are as follows: $f_{\rm local}^{\rm NL} = 2.7 \pm 5.8$, $f_{\rm equil}^{\rm NL} = -42 \pm 75$ and $f_{\rm ortho}^{\rm NL} = -25 \pm 39$. MF-based analysis using Planck data produces results that are consistent with a null-hypothesis for the local model of NG. While the estimation of primordial NG may be the primary motivation behind the study of MFs in the context of CMB, they have also been applied to probe gravity-induced secondary NG using weak-lensing convergence or κ-maps (Matsubara & Jain 2001; Taruya et al. 2002). One of the main motivations behind studying various alternatives that probe primordial NG has to do with issues related to estimation. Different probes are affected differently by different contamination such as the presence of foreground or secondary NG. The methods based on multispectra that are typically employed for the estimation of NG use a Fourier (or harmonic) space approach. On the other hand, the techniques developed for estimation of MFs are traditionally applied in real space. Matsubara (2003) obtained a closed-form expression for MFs in D dimensions using a perturbative

[5] http://www.physics.princeton.edu/act/
[6] http://pole.uchicago.edu/

expansion in terms of various orders of multispectra. At the lowest order, a departure from Gaussianity is characterized by three different skewness parameters $S^{(0)}$, $S^{(1)}$, $S^{(2)}$. The skewness parameter $S^{(0)}$ is the ordinary skewness that is most commonly used in various studies of NG for projected surveys as well as in 3D. The other set of skewness parameters are defined in terms of different cubic statistics that are constructed from the original data using differential operators. The purpose of this paper is to retain more of the details of the NG in these methods, in order to aid in determining the source of NG. This is very similar to the approach of Munshi & Heavens (2010), who devised an optimal compression of bispectrum data which retained enough information to determine point source and lensing–integrated Sachs–Wolfe (ISW) contributions to *Planck* data (Planck Collaboration 2013).

This paper is organized as follows. In Section 2, we review the formalism of MFs. In Section 3, we focus on the one-point estimators, the generalized skewness, and their links to MFs. In Section 4, real-life issues such as the mask and noise are discussed and estimators are designed for estimation of the MFs using a pseudo-$\mathcal{C}_\ell$ based approach. In Section 5, we provide generic result to reconstruct the MFs using modal decomposition of the bi- or trispectrum. In Section 6, we extend the concept of skew-spectrum to odd-parity bispectra. In Section 7, we present our results of morphological analysis in the needlet basis. We relate the skew-spectrum defined in the needlet basis with that in harmonic domain. Finally, Section 8 is left for discussion and Section 9 for conclusions.

In Appendix A various early Universe models and their predictions for the lower order multispectra are presented. In Appendix B, the corrections to the lowest order in NG are discussed. These corrections are related to estimation of trispectra.

Throughout in this paper a *WMAP*7 (Larson et al. 2010) background cosmology will be used for computation of various spectra. Unless specified, the values of the normalization parameters $f_{\rm NL}^{\rm loc}$, $f_{\rm NL}^{\rm equi}$, $f_{\rm NL}^{\rm en}$ and $f_{\rm NL}^{\rm orth}$ (to be defined later), are set to unity.[7]

We will consider two different experimental setups. For *Planck*, we take the 143 GHz channel and for EPIC we take the 150 GHz channel. The beams for these experiments are $\theta_s = 7.1$ arcmin and $\theta_s = 5$ arcmin. The pixel areas for *Planck* and EPIC are given by $\Omega_{\rm pix} = 0.0349$ and $\Omega_{\rm pix} = 0.0002$. The noise per pixel for *Planck* is $\sigma_{\rm pix} = 2.2 \times 10^{-6}$ and for EPIC is given by $\sigma_{\rm pix} = 8.0 \times 10^{-6}$.

2 FORMALISM

The MFs are well-known morphological descriptors which are used in the study of random fields. Morphological properties are the properties that remain invariant under rotation and translation (see Hadwiger 1959 for a more formal introduction). They are defined over an excursion set Σ, for a given threshold ν. The three MFs that are defined for two-dimensional (2D) studies can be expressed as

$$\mathcal{V}_0(\nu) = \int_\Sigma {\rm d}a; \quad \mathcal{V}_1(\nu) = \frac{1}{4}\int_{\partial\Sigma} {\rm d}l; \quad \mathcal{V}_2(\nu) = \frac{1}{2\pi}\int_{\partial\Sigma} \kappa\, {\rm d}l. \tag{2}$$

Here da and dl are the elements for the excursion set Σ and its boundary $\partial\Sigma$. The MFs $\mathcal{V}_k(\nu)$ correspond to the area of the excursion set Σ, the length of its boundary $\partial\Sigma$ and the integral curvature along its boundary, which is related to the genus g and hence the Euler characteristic χ. In our analysis, we will consider a smoothed random field (e.g. CMB temperature distribution on the surface of the sky) $\Psi(\hat{\Omega}) = \delta T(\hat{\Omega})/T_0$ with mean $\langle\Psi(\hat{\Omega})\rangle = 0$ and variance $\sigma_0^2 = \langle\Psi^2(\hat{\Omega})\rangle$, for a generic 2D weakly non-Gaussian random field Ψ. The spherical harmonic decomposition using $Y_{\ell m}(\hat{\Omega})$ as a basis function, $\Psi(\hat{\Omega}) = \sum_{\ell m}\Psi_{\ell m}Y_{\ell m}(\hat{\Omega})$ can be used to define the power spectrum $\mathcal{C}_l$ which is sufficient characterization of a Gaussian field $\langle\Psi_{\ell m}\Psi^*_{\ell' m'}\rangle = \mathcal{C}_\ell\delta_{\ell\ell'}\delta_{mm'}$. For a non-Gaussian field, the higher order statistics such as the bi- or trispectrum can describe the resulting mode–mode coupling. Alternatively, the topological measures such as MFs which include the Euler characteristic or genus can be employed to quantify deviation from Gaussianity. At the leading order, the MFs can be constructed completely from the knowledge of the bispectrum alone. We will be studying the MFs defined over the surface of the celestial sphere, but equivalent results can be obtained in 3D using a Fourier decomposition (Munshi 2013, in preparation). The notation and analytical results in this section are being kept generic; however, they will be specialized to the case of the CMB sky in subsequent discussions. Using a perturbative series expansion in the field rms, σ_0, the MFs denoted as $\mathcal{V}_k(\nu)$ for a threshold $\nu = \Psi/\sigma_0$ can be expressed as follows (Matsubara 2003):

$$\mathcal{V}_k(\nu) = \frac{1}{(2\pi)^{(k+1)/2}}\frac{\omega_2}{\omega_{2-k}\omega_k}\exp\left(-\frac{\nu^2}{2}\right)\left(\frac{\sigma_1}{\sqrt{2}\sigma_0}\right)^k\left[v_k^{(1)}(\nu) + v_k^{(2)}(\nu)\sigma_0 + v_k^{(3)}(\nu)\sigma_0^2 + v_k^{(4)}(\nu)\sigma_0^3 + \cdots\right]; \tag{3}$$

$$v_k^{(1)}(\nu) = \mathcal{H}_{k-1}(\nu); \quad v_k^{(2)}(\nu) = \left[\left\{\frac{1}{6}S^{(0)}\mathcal{H}_{k+2}(\nu) + \frac{k}{3}S^{(1)}\mathcal{H}_k(\nu) + \frac{k(k-1)}{6}S^{(2)}\mathcal{H}_{k-2}(\nu)\right\}\right]; \tag{4}$$

$$\sigma_j^2 = \frac{1}{4\pi}\sum_\ell \Pi_\ell^j\,\Xi_\ell\,\mathcal{C}_\ell\,b_\ell^2; \quad \Pi_\ell = \ell(\ell+1); \quad \Xi_\ell = (2\ell+1). \tag{5}$$

The constant ω_k introduced above is the volume of the unit sphere in k-dimensions: $w_k = \frac{\pi^{k/2}}{\Gamma(k/2+1)}$, and the skewness parameters $S^{(i)}$ are defined below in equation (7). In 2D, we will only need $\omega_0 = 1$, $\omega_1 = 2$ and $\omega_2 = \pi$ and the lowest order Hermite polynomials $\mathcal{H}_k(\nu)$ are

[7] The techniques presented in this paper have already been used in the context of CMB secondaries (Munshi, Coles & Heavens 2013), frequency-cleaned thermal Sunyaev–Zeldovich (tSZ) map (Munshi et al. 2012a), weak-lensing convergence maps (Munshi et al. 2012b) as well as in galaxy redshift surveys (Pratten & Munshi 2012).

listed below:

$$\mathcal{H}_{-1}(\nu) = \sqrt{\frac{\pi}{2}}\exp\left(\frac{\nu^2}{2}\right)\mathrm{erfc}\left(\frac{\nu}{\sqrt{2}}\right); \quad \mathcal{H}_0(\nu) = 1, \quad \mathcal{H}_1(\nu) = \nu,$$
$$\mathcal{H}_2(\nu) = \nu^2 - 1, \quad \mathcal{H}_3(\nu) = \nu^3 - 3\nu, \qquad \mathcal{H}_4(\nu) = \nu^4 - 6\nu^2 + 3;$$
$$\mathcal{H}_n(\nu) = (-1)^n \exp\left(\frac{\nu^2}{2}\right)\frac{\mathrm{d}^n}{\mathrm{d}\nu^n}\exp\left(-\frac{\nu^2}{2}\right). \tag{6}$$

The MFs consist of two distinct contributions: one, which is independent of the three different skewness parameters $S^{(0)}$, $S^{(1)}$, $S^{(2)}$, signifies the MFs for a Gaussian random field, and are denoted by $v_k^{(1)}(\nu)$; the other contribution $v_k^{(2)}(\nu)$ represents the departure from Gaussian statistics and depends on the generalized skewness parameters. The next-to-leading-order corrections $v_k^{(3)}(\nu)$ depend on the generalized kurtosis parameters and will be discussed in more detail in Appendix B. Various moments σ_j that appear in equation (5) can be expressed in terms of the power spectrum $\mathcal{C}_\ell$ and the observational beam $b_\ell(\theta_s)$ (the full width at half-maximum or FWHM is denoted by θ_s). The moments that will mostly be used are $\sigma_0^2 = \langle\Psi^2\rangle$ and $\sigma_1^2 = \langle(\nabla\Psi)^2\rangle$.

The real-space expressions for the triplets of skewness $S^{(i)}$, which appear in the expressions for the MFs, are given below. These are natural generalizations of the ordinary skewness $S^{(0)}$ that is used in many cosmological studies, but are constructed from different cubic combinations

$$S^{(0)} \equiv \frac{S^{(\Psi^3)}}{\sigma_0^4} = \frac{\langle\Psi^3\rangle}{\sigma_0^4}; \quad S^{(1)} \equiv -\frac{3}{4}\frac{S^{(\Psi^2\nabla^2\Psi)}}{\sigma_0^2\sigma_1^2} = -\frac{3}{4}\frac{\langle\Psi^2\nabla^2\Psi\rangle}{\sigma_0^2\sigma_1^2}; \quad S^{(2)} \equiv -3\frac{S^{(\nabla\Psi.\nabla\Psi\nabla^2\Psi)}}{\sigma_1^4} = -3\frac{\langle(\nabla\Psi).(\nabla\Psi)(\nabla^2\Psi)\rangle}{\sigma_1^4}. \tag{7}$$

These one-point generalized skewness parameters are plotted in Fig. 1 for various models of NG. The expressions in the harmonic domain are more useful in the context of CMB studies where we will be recovering them from a masked sky using analytical tools that are commonly used for power spectrum analysis. The expressions for the MFs in equation (5) that we have discussed, depend on the one-point cumulants $S^{(i)}$. However, it is possible to define power spectra associated with each of these skewness parameters following a procedure similar to that developed in Munshi & Heavens (2010). This is one of the main motivations behind generalizing the concept of MFs, each of which is a number, to a set of power spectra. As an illustration of the power of the skew-$\mathcal{C}_\ell$s see Planck Collaboration (2013) which demonstrates detection of ISW–lensing and point source non-Gaussianities.

The series expansion for the MFs can be extended beyond the level of the bispectrum. The next-to-leading-order corrections terms are related to trispectra of the original map. These corrections are expected to be subdominant in the context of CMB studies for the entire range of angular scales being probed. However, if the primordial bispectrum is negligible, as seems to be the case, these terms may play an important role in shaping the topology of the CMB sky. In addition, lensing-induced topology change appears only at the level of trispectrum.

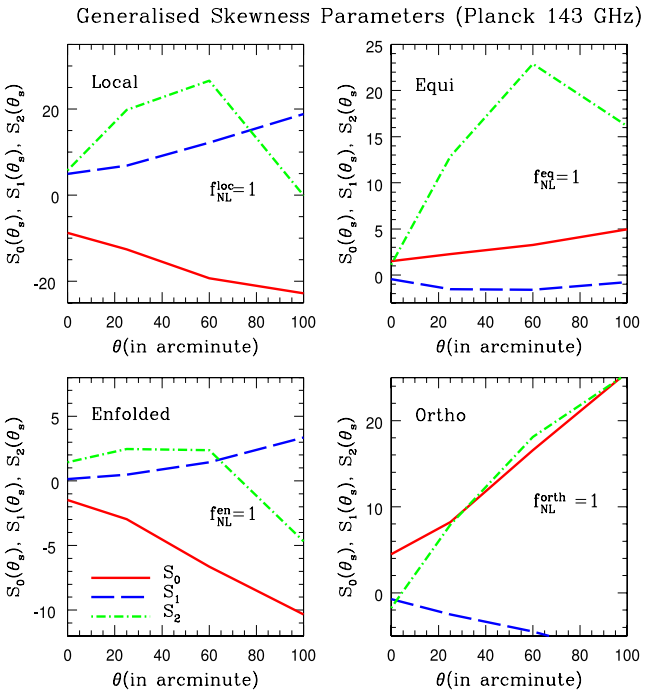

Figure 1. The generalized skewness parameters $S^{(0)}$ (solid lines), $S^{(1)}$ (short dashed lines) and $S^{(2)}$ (long dashed lines), defined in equation (7), are plotted as a function of the beam FWHM θ_s (in arcminute). The upper-left panel corresponds to the *local* model and the upper-right panel correponds to the *equilateral* model, whereas the lower-left and lower-right panels correspond to *enfolded* and *orthogonal model*, respectively. The normalization parameter $f_{\rm NL}$ describing various models of NG are set to unity $f_{\rm NL} = 1$. The experimental setup corresponds to that of the *Planck* 143 GHz channel.

The results here correspond to maps of temperature, which is a spin-0 object. It is possible to extend these results to the case of polarization analysis, i.e. for spin-2 fields. Such results will also be relevant in the context of weak-lensing shear and flexions. A detailed analysis will be presented elsewhere.

3 THE TRIPLETS OF SKEW-SPECTRA AND LOWEST-ORDER CORRECTIONS TO GAUSSIAN MFs

The skew-spectra are cubic statistics that are constructed by cross-correlating two different fields. One of the fields used is a composite field, typically a product of two maps, either in its original form or constructed by means of relevant differential operations. The second field will typically be a single field but may be constructed by applying various differential operators. These three skewness parameters contribute to the three MFs that we will consider in 2D.

The first of the skew-spectra was studied by Cooray (2001) and later by Munshi & Heavens (2010) and is related to the commonly used skewness. The skewness in this case is constructed by cross-correlating the squared map $\Psi^2(\hat{\Omega})$ with the original map $\Psi(\hat{\Omega})$. The second skew-spectrum is constructed by cross-correlating the squared map $\Psi^2(\hat{\Omega})$ with $\nabla^2\Psi(\hat{\Omega})$. Analogously, the third skew-spectrum represents the cross-spectra that can be constructed using $\nabla\Psi(\hat{\Omega})\cdot\nabla\Psi(\hat{\Omega})$ and $\nabla^2\Psi(\hat{\Omega})$:

$$S_\ell^{(0)} \equiv \frac{1}{\sigma_0^4} S_\ell^{(\Psi^2,\Psi)} \equiv \frac{1}{\sigma_0^4}\frac{1}{\Xi_\ell}\sum_m \mathrm{Real}(\langle [\Psi]_{\ell m}[\Psi^2]^*_{\ell m}\rangle) = \frac{1}{\sigma_0^4}\sum_{\ell_1\ell_2} B_{\ell\ell_1\ell_2} J_{\ell\ell_1\ell_2} b_\ell b_{\ell_1} b_{\ell_2}; \tag{8}$$

$$\begin{aligned} S_\ell^{(1)} &\equiv -\frac{3}{4}\frac{1}{\sigma_0^2\sigma_1^2} S_\ell^{(\Psi^2,\nabla^2\Psi)} \equiv -\frac{3}{4\sigma_0^2\sigma_1^2}\frac{1}{\Xi_\ell}\sum_m \mathrm{Real}(\langle [\nabla^2\Psi]_{\ell m}[\Psi^2]^*_{\ell m}\rangle) \\ &= -\frac{3}{4\sigma_0^2\sigma_1^2}\sum_{\ell_1\ell_2}\frac{1}{3}\left(\Pi_\ell + \Pi_{\ell_1} + \Pi_{\ell_2}\right) B_{\ell\ell_1\ell_2} J_{\ell\ell_1\ell_2} b_{\ell_1} b_{\ell_2} b_{\ell_3}; \end{aligned} \tag{9}$$

$$\begin{aligned} S_\ell^{(2)} &\equiv -\frac{3}{\sigma_1^4} S_\ell^{(\nabla\Psi\cdot\nabla\Psi,\nabla^2\Psi)} \equiv -\frac{3}{\sigma_1^4}\frac{1}{\Xi_\ell}\sum_m \mathrm{Real}(\langle [\nabla\Psi\cdot\nabla\Psi]_{\ell m}[\nabla^2\Psi]^*_{\ell m}\rangle) \\ &= \frac{3}{\sigma_1^4}\sum_{\ell_1\ell_2}\frac{1}{3}\left[(\Pi_\ell + \Pi_{\ell_1} - \Pi_{\ell_2})\frac{\Pi_{\ell_2}}{2} + \text{cyc.perm.}\right] B_{\ell\ell_1\ell_2} J_{\ell\ell_1\ell_2} b_\ell b_{\ell_1} b_{\ell_2}; \end{aligned} \tag{10}$$

$$J_{\ell_1\ell_2\ell_3} \equiv \frac{1}{\Xi_{\ell_3}} I_{\ell_1\ell_2\ell_3} = \sqrt{\frac{\Xi_{\ell_1}\,\Xi_{\ell_2}}{4\pi\;\Xi_{\ell_3}}} \begin{pmatrix} \ell_1 & \ell_2 & \ell_3 \\ 0 & 0 & 0 \end{pmatrix}. \tag{11}$$

The more usual skewness parameters are related to the skew-spectra by

$$S^{(i)} = \frac{1}{4\pi}\sum_\ell \Xi_\ell\; S_\ell^{(i)}. \tag{12}$$

The bispectrum $B_{\ell_1\ell_2\ell_3}$ used here defines the three-point correlation function in the harmonic domain. In general, a reduced bispectrum $b_{\ell_1\ell_2\ell_3}$ is commonly used:

$$\langle \Psi_{\ell_1 m_1}\Psi_{\ell_2 m_2}\Psi_{\ell_3 m_3}\rangle_c = \begin{pmatrix} \ell_1 & \ell_2 & \ell_3 \\ m_1 & m_2 & m_3 \end{pmatrix} B_{\ell_1\ell_2\ell_3}; \qquad B_{\ell_1\ell_2\ell_3} = I_{\ell_1\ell_2\ell_3} b_{\ell_1\ell_2\ell_3}. \tag{13}$$

This set of equations constitutes one of the main results in this paper. b_l represents the experimental beam $b_\ell \equiv b_\ell(\theta_s) = \exp\{-\ell(\ell+1)\sigma_b^2/2\}$ with $\sigma_b = \theta_s/\sqrt{8\ln 2}$ for a Gaussian beam. Each of these spectra probes the same bispectrum $B_{\ell\ell_1\ell_2}$ with different weights for individual triplets of modes that specifies the bispectrum (ℓ, ℓ_1, ℓ_2). Each triplets of modes specifies a triangle in the harmonic domain. The skew-spectra sum over all possible configurations of the bispectrum keeping one of its sides ℓ fixed. For each individual, choice of ℓ we can compute the skew-spectra $S_\ell^{(i)}$.

The expression for the optimum skew-spectrum estimator $S_\ell^{\rm opt}$ and its one-point counterpart or the optimum skewness $S^{\rm opt}$ are given by (Munshi & Heavens 2010)

$$S_l^{\rm opt} = \frac{1}{2\ell+1}\sum_{\ell_1\ell_2}\frac{\hat{B}_{\ell\ell_1\ell_2} B_{\ell\ell_1\ell_2}}{\mathcal{C}_\ell \mathcal{C}_{\ell_1}\mathcal{C}_{\ell_2}}; \qquad S^{\rm opt} = \sum_\ell (2\ell+1) S_\ell^{\rm opt}. \tag{14}$$

Here $\hat{B}_{\ell\ell_1\ell_2}$ is the bispectrum estimated from the data and $B_{\ell\ell_1\ell_2}$ is the theoretical model under consideration. The optimum estimator for various models that we consider is presented in Fig. 2.

An alternative is to formulate the analysis in real space, using the two-to-one *cumulant correlators* $S^{(i)}(\theta_{12})$:

$$S^{(0)}(\theta_{12}) \equiv \frac{1}{\sigma_0^4}\; S^{\Psi^2,\Psi}\;(\theta_{12}) \equiv \frac{1}{\sigma_0^4}\langle \Psi^2(\hat{\Omega}_1)\Psi(\hat{\Omega}_2)\rangle = \frac{1}{4\pi}\sum_l \Xi_\ell\; S_\ell^{(0)} P_\ell(\cos\theta_{12}); \tag{15}$$

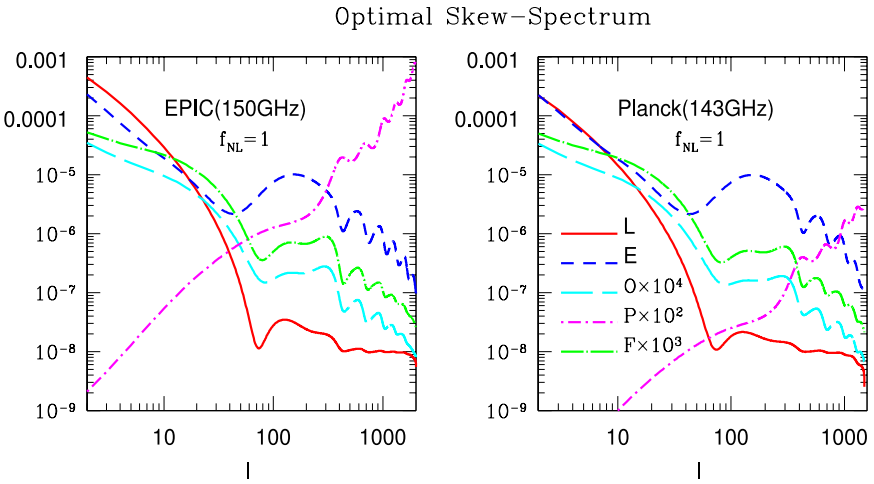

Figure 2. The signal expected from the optimum estimator (see equation 14 for definition) for the skew-spectra $\mathcal{S}_\ell^{\rm opt}$ is shown as a function of the angular harmonics ℓ. The left-hand panel correspond to EPIC (150 GHz channel) and the right-hand panel correspond to *Planck* (143 GHz channel). The solid, short dashed, long dashed, dot–short dashed and dot–long dashed lines correspond to local (L), equilateral (E), orthogonal (O) and enfolded (F) and point sources (P), respectively. We have scaled some of the models as depicted. The parameter $f_{\rm NL}$ is set to unity for each of these models.

$$S^{(1)}(\theta_{12}) \equiv -\frac{3}{4\sigma_0^2\sigma_1^2}\, S^{\Psi^2,\nabla^2\Psi}(\theta_{12}) \equiv -\frac{3}{4\sigma_0^2\sigma_1^2}\langle\Psi^2(\hat{\Omega}_1)\nabla^2\Psi(\hat{\Omega}_2)\rangle = \frac{1}{4\pi}\sum_l \Xi_\ell\; S_\ell^{(1)} P_\ell(\cos\theta_{12}); \tag{16}$$

$$S^{(2)}(\theta_{12}) \equiv -\frac{3}{\sigma_1^4} S^{\nabla\Psi\cdot\nabla\Psi,\nabla^2\Psi}(\theta_{12}) \equiv -\frac{3}{\sigma_1^4}\langle\nabla\Psi(\hat{\Omega}_1)\cdot\nabla\Psi(\hat{\Omega}_1)\nabla^2\Psi(\hat{\Omega}_2)\rangle = \frac{1}{4\pi}\sum_l \Xi_\ell\; S_\ell^{(2)} P_\ell(\cos\theta_{12}); \tag{17}$$

$$S^{\rm opt}(\theta_{12}) \equiv \sum_\ell (2\ell+1) S_\ell^{\rm opt} P_\ell(\cos\theta_{12}). \tag{18}$$

Here, θ_{12} represents the angle of separation between $\hat{\Omega}_1$ and $\hat{\Omega}_2$, and P_ℓ is a Legendre polynomial. In the zero angular separation limit $\theta_{12} = 0$, the two-point objects reduce to their one-point counterparts $S^{(0)}(0) \equiv S^{(0)}$; $S^{(1)}(0) \equiv S^{(1)}$ and $S^{(2)}(0) \equiv S^{(2)}$, respectively. Similar construction is possible for the case of optimum estimator too. In addition to the real-space description and its harmonic counterpart, the needlet basis provides an intermediate choice. We will consider the skew-spectra in needlet basis in Section 7.

The extraction of skew-spectra from data is relatively straightforward. It consists of construction the relevant maps in real space, either by algebraic or differential operation, and then cross-correlating them in the multipole space. The issues related to mask and noise will be dealt with in later sections. We will show that even in the presence of a mask, the computed skew spectra can be inverted to give an unbiased estimate of all-sky skew-spectra, with noise only affecting the scatter.

To derive the above expressions, we first express the spherical harmonic expansion of the fields $\nabla^2\Psi(\hat{\Omega})$, $\nabla\Psi(\hat{\Omega})\cdot\nabla\Psi(\hat{\Omega})$ and $\Psi^2(\hat{\Omega})$ in terms of the harmonics of the original fields, Ψ_{lm}. These expressions involve the $3j$ functions as well as factors that depend on various ℓ_i-dependent weight factors. These aspects and related issues have already been dealt with in previous publications in different contexts (Munshi et al. 2012a,b).

We can the define the power spectrum associated with the MFs through the following third-order expression:

$$v_k^{(2)}(\nu) = \sum_\ell \Xi_\ell\, [v_k^{(2)}]_\ell(\nu) = \frac{1}{6}\sum_\ell \Xi_\ell \left\{ S_\ell^{(0)}\mathcal{H}_{k+2}(\nu) + \frac{k}{3} S_\ell^{(1)}\mathcal{H}_k(\nu) + \frac{k(k-1)}{6} S_\ell^{(2)}\mathcal{H}_{k-2}(\nu) + \cdots \right\}. \tag{19}$$

The three skewness parameters define the triplets of MFs. At the level of two-point statistics, in the harmonic domain we have three power-spectra associated with MFs $v_k^{(2)}$ that depend on the three skew-spectra we have defined. We will show later in this paper that the fourth-order correction terms too have a similar form with an additional monopole contribution that can be computed from the lower order one-point terms such as the three skewness defined here. The result presented here is important and implies that we can study the contributions to each of the MFs $v_k(\nu)$ as a function of harmonic mode ℓ. This is an especially significant result as various forms of NG will have different ℓ dependence and hence they can potentially be distinguished. The ordinary MFs add contributions from individual ℓ modes and hence have less power in differentiating various contributing sources of NG. This is one of main motivations to extend the concept of MFs (single numbers) to one-dimensional objects similar to the power spectrum.

In Fig. 3, we have presented the three different skew-spectra for the local model as a function of the harmonics ℓ. The skew-spectra for a generic bispectrum are defined in equations (8)–(10). The skew-spectra are sensitive to the smoothing b_ℓ; moreover, the skew-spectra at a given ℓ depend on the bispectrum defined over the entire range of ℓ being probed. The skew-spectra for equilateral, orthogonal and enfolded model are presented in Fig. 4, Fig. 5 and Fig. 6, respectively. The normalization parameters for these plots are set to be equal to unity; i.e.

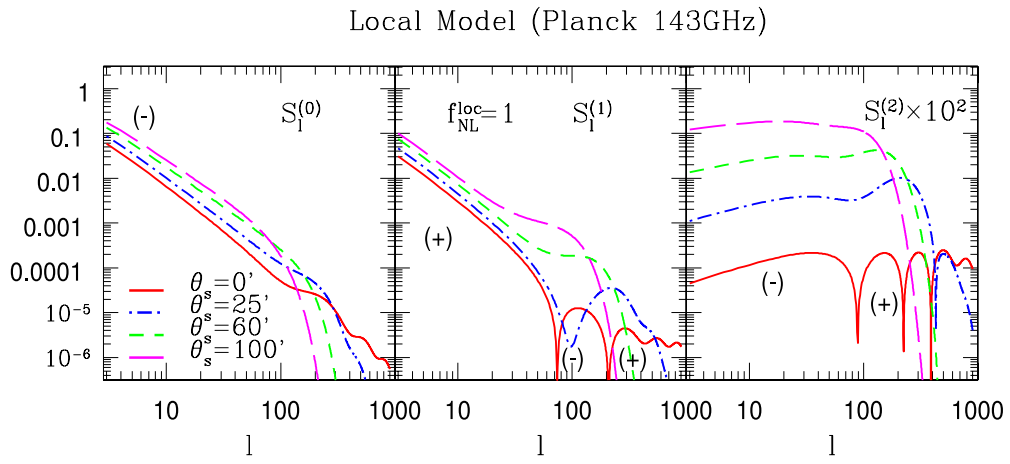

Figure 3. The skew-spectra $S_\ell^{(0)}$ (left-hand panel), $S_\ell^{(1)}$(middle panel) and $S_\ell^{(2)}$ (right-hand panel) are plotted for various smoothing beams (see equation 12) as a function of the harmonics ℓ. The model for the primordial NG is assumed to be a local model for these plots equation (A3). The underlying cosmology is assumed to be that of *WMAP*7. The FWHM for the four beams considered are $\theta_s = 0$ arcmin (solid), 25 arcmin (dot–dashed), 50 arcmin (small dashed) and 100 arcmin (long dashed). The parameter $f_{\rm NL}^{\rm loc}$ describing the normalization of local model of NG is set to unity $f_{\rm NL}^{\rm loc} = 1$, and the resolution is set at $\ell_{\rm max} = 1500$. To extract the skewness parameters, we use the relationship $S^{(i)} = \frac{1}{4\pi}\sum_\ell \Xi_\ell S_\ell^{(i)}$. The experimental noise corresponds to that of *Planck* 143 GHz channel.

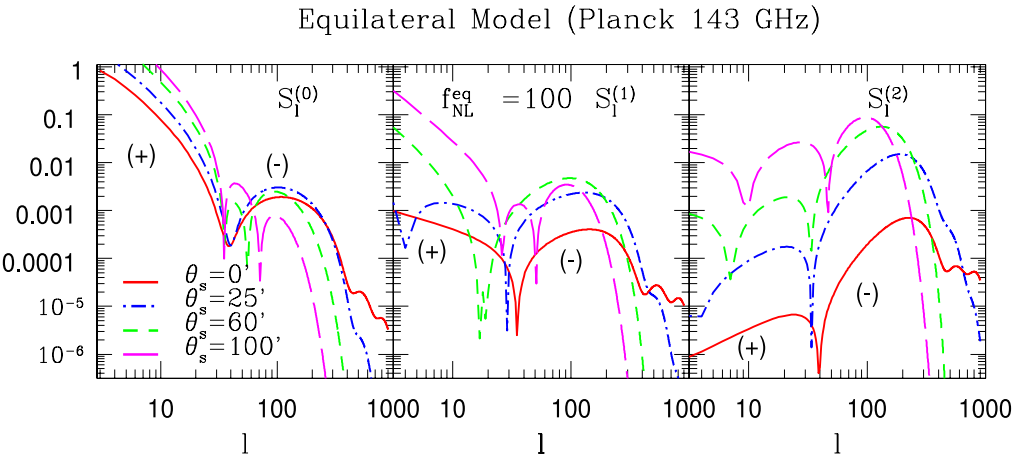

Figure 4. Same as previous figure but for the equilateral model of primordial NG as defined in equation (A6). The choice of smoothing angular scales (beam) are the same as previous figure. The normalization parameter for the equilateral bispectrum $f_{\rm NL}^{\rm eq}$ is fixed at $f_{\rm NL}^{\rm eq} = 100$.

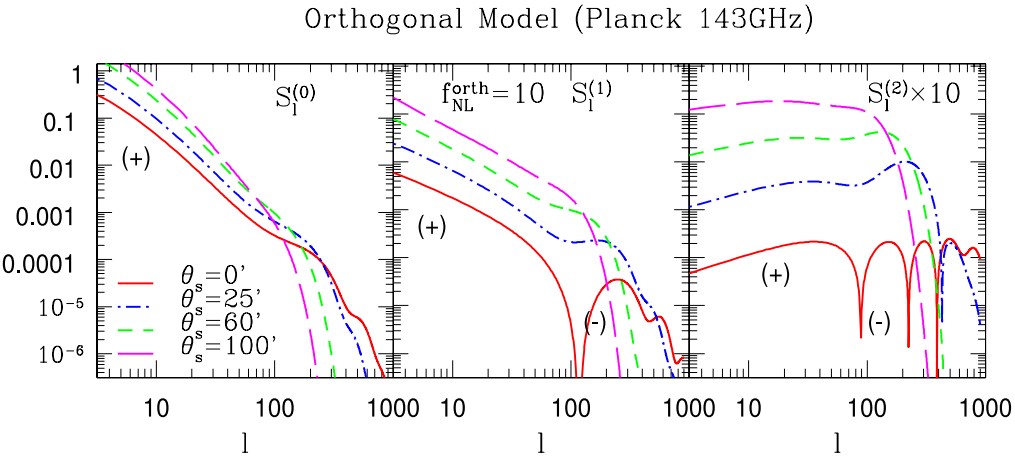

Figure 5. Same as previous figure but for the orthogonal model of primordial NG. The choice of smoothing angular scales (beam) are the same as previous figure. The value of the normalization parameter for the orthogonal model of bispectrum $f_{\rm NL}^{\rm orth}$ is fixed at $f_{\rm NL}^{\rm orth} = 10$.

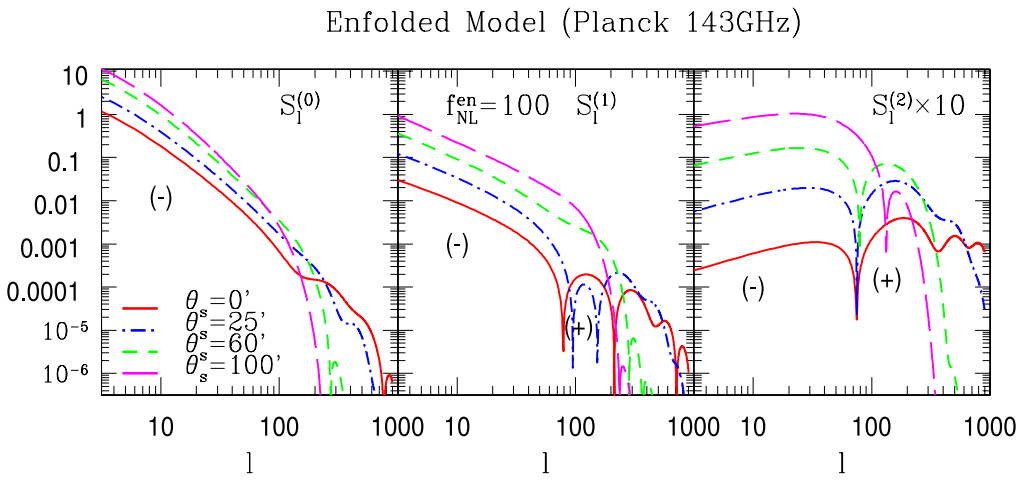

Figure 6. Same as previous figure but for the enfolded model of primordial NG. The choice of smoothing angular scales (beam) are the same as previous figure. The normalization parameter for the enfolded bispectrum $f_{\rm NL}^{\rm en}$ is fixed at $f_{\rm NL}^{\rm en} = 100$.

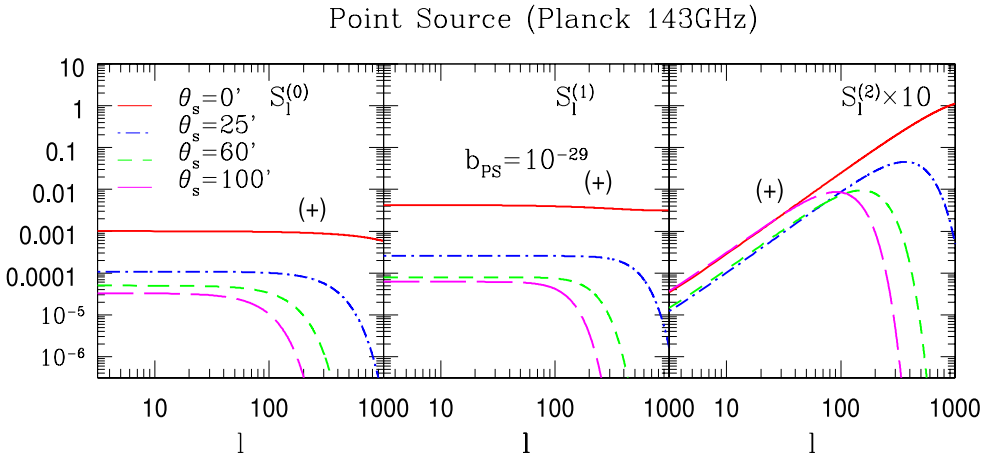

Figure 7. Same as previous figures but for uncorrelated point sources. For the point sources, we have taken $b_{\rm PS} = 10^{-29}\ \mu K^3$. The panels represent the three different skew-spectra $S_\ell^{(0)}$ (left-hand panel), $S_\ell^{(1)}$ (middle panel) and $S_\ell^{(2)}$ (right-hand panel), respectively. The skew-spectra are sensitive to the resolution of the maps being analysed as they are integrated measures. This is related to the fact that its value at a specific harmonics ℓ takes contribution from all possible modes, i.e. the entire range of ℓ values. The point source contributions dominate the primordial NG at high ℓ.

we take $f_{\rm NL}^{\rm loc} = 1$ and similarly for other models. The skew-spectra will scale linearly with these $f_{\rm NL}$ parameters. In addition to the amplitude of the skew-spectra, comparing the figures we can see that equilateral model produced the most distinct type of skew-spectra which is very different from all other models. The skew-spectra of other models too have very different signature especially at high ℓs.

For our computation of the MFs, we have used the freely available software archive SHTOOLS.[8] In particular, we used its Wigner-3j symbol routine that provides accurate numerical convergence, especially for high values of ℓ. We used a parallel implementation of equations (8)–(10) for evaluation of the skew-spectra. For the separable models of bispectra considered here two hours of computations were required on 20 CPUs. The computations were dominated by evaluation of 3j symbols.

The unresolved point sources are mostly unresolved galaxies, i.e. radio galaxies not emitting strongly enough for their individual detection; which emit in radio frequencies via the synchrotron process or dusty starburst galaxies which are observed via thermal emission of their dust. The integrated diffuse emission from all galaxies constitute what is commonly known as the cosmic infrared background. The brightest point sources can be removed using an appropriate mask. The unresolved point sources, however, do contribute to the CMB bispectrum, and in general they will be clustered and require more detailed modelling. The skew-spectra for Poisson-distributed point sources are plotted in Fig. 7. The specific model for the bispectrum that we consider is given in equation (20), and the point sources are expected to dominate at higher ℓ values. The normalization for the point source bispectrum is set by the parameter $b_{\rm PS}$. Assuming point sources are not clustered and can be represented as a Poissionian distribution we can write the corresponding bispectrum as

$$b_{\ell_1\ell_2\ell_3} = b_{\rm PS}. \tag{20}$$

[8] shtools.ipgp.fr

The exact value of the amplitude $b_{\rm PS}$ depends on the limiting flux used in a specific survey. In our study, we have taken $b_{\rm PS} = 10^{-29}\ \mu{\rm K}^3$. The results of our computations are plotted in Fig. 7. We have considered four different Gaussian beams as indicated $\theta_s = 10$, 25, 50 and 100 arcmin. The skew-spectra $S_\ell^{(2)}$, which puts more weights on smaller angular scales, is more dominated by point source contributions. The cumulant correlators introduced in equations (15)–(17) are depicted in Fig. B1 for four different models that we have considered.

Next, we consider the higher order corrections to the MFs. These corrections take contributions from the trispectrum. Corrections to the individual MFs can be expressed in terms of a set of four kurtosis terms which are formed from the trispectra. These kurtosis terms are one-point estimators and they differ in the way they sample the individual modes of the trispectra defined by the quadruplet of harmonic number $\{\ell_i\}$; $i = 1, 2, 3, 4$. These generalized kurtosis parameters (denoted by $K^{(i)}$) can be generalized to *kurt-spectra*, denoted as $K_\ell^{(i)}$, in a manner very similar to the skew-spectra. These kurt-spectra can be used to express the next-order corrections to the power spectra associated with MFs.

4 ESTIMATORS AND THEIR COVARIANCE

The results derived above correspond to the all-sky and no-noise situation. However, in reality often we have to deal with issues that are related to the presence of a mask and (inhomogeneous) noise. To correct for the effect of a mask and the noise we will follows the pseudo-$\mathcal{C}_\ell$ method devised by Hivon et al. (2002) for power spectrum analysis and later developed by Munshi et al. (2011b) for analysing the skew spectra and kurt-spectrum (Munshi et al. 2011a).

The partial sky coverage introduces mode–mode coupling in the harmonic domain and individual masked harmonics become linear combinations of all-sky harmonics. The coefficients for this linear transformation depend on the mask through its harmonic coefficients. We will devise a method that can be used to correct for the mode–mode coupling. If we have a generic field $A(\hat\Omega)$ and $B(\hat\Omega)$, we denote their harmonic decomposition in the presence of a mask $w(\hat\Omega)$ as $\tilde A_{\ell m}$ and $\tilde B_{\ell m}$. Note that the mask is completely general and our results do not depend on any specific symmetry requirements such as the azimuthal symmetry. The fields A and B may correspond to any of the fields we have considered above. In a generic situation A and B will denote composite fields and the harmonics $A_{\ell m}$ and $B_{\ell m}$ will correspond to any of the harmonics used in equations (8)–(10).

$$\tilde A_{\ell m} = \int {\rm d}\hat\Omega Y^*_{\ell m}(\hat\Omega)\, w(\hat\Omega)\, A(\hat\Omega); \qquad \tilde B_{\ell m} = \int {\rm d}\hat\Omega\, Y^*_{\ell m}(\hat\Omega)\, w(\hat\Omega) B(\hat\Omega); \tag{21}$$

$$\tilde A_{\ell m} = \sum_{\ell_i m_i} (-1)^m\, I_{\ell\ell_1\ell_2} \begin{pmatrix} \ell_1 & \ell_2 & \ell \\ m_1 & m_2 & -m \end{pmatrix} w_{\ell_1 m_1} A_{\ell_2 m_2}; \quad \tilde B_{\ell m} = \sum_{\ell_i m_i} (-1)^m I_{\ell\ell_1\ell_2} \begin{pmatrix} \ell_1 & \ell_2 & \ell \\ m_1 & m_2 & -m \end{pmatrix} w_{\ell_1 m_1} B_{\ell_2 m_2}. \tag{22}$$

The above expression relates the masked harmonics denoted by $\tilde A_{\ell m}$ and $\tilde B_{\ell m}$ with their all-sky counterparts $A_{\ell m}$ and $B_{\ell m}$, respectively. In their derivation, we use the Gaunt integral to express the overlap integrals involving three spherical harmonics in terms of the $3j$ symbols (Edmonds 1968). The expressions also depend on the harmonics of the mask $w_{\ell m}$. If we now denote the (cross) power spectrum constructed from the masked harmonics and denote it by $\tilde S_\ell$ and its all-sky counterpart by S_ℓ, we can write

$$\tilde S_\ell^{A,B} = \frac{1}{\Xi_\ell} \sum_m \tilde A_{\ell m} \tilde B^*_{\ell m}; \quad \tilde S_\ell^{A,B} = \sum_{\ell'} \mathbf{M}_{\ell\ell'} S_\ell^{A,B}; \quad \mathbf{M}_{\ell\ell'} = \frac{1}{\Xi_\ell} \sum_{\ell''} I^2_{\ell\ell'\ell''} |w_{\ell''}|^2; \quad \{A, B\} \in \left\{\Psi, \Psi^2, (\nabla\Psi\cdot\nabla\Psi), \nabla^2\Psi\right\}. \tag{23}$$

Here, w_ℓ represents the power spectrum of the mask $w(\hat\Omega)$, i.e. $w_\ell = \frac{1}{2\ell+1}\sum_{m=-\ell}^{m=\ell} w_{\ell m} w^*_{\ell m}$.

In the above derivation, we have used the orthogonality properties of the $3j$ symbols. It is interesting to note that the *convolved* power spectrum estimated from the masked sky is a linear combination of all-sky spectra and depends only on the power spectra of the mask used. The linear transform is encoded in the mode–mode coupling matrix $\mathbf{M}_{\ell\ell'}$ which is constructed from the knowledge of the power spectrum of the mask. In certain situations where the sky coverage is low, the direct inversion of the mode mixing matrix $\mathbf{M}$ may not be possible due to its singularity and binning may be essential. Based on these results, it is possible to define an unbiased estimator that we denote by $\hat S_\ell^{A,B}$. The noise due to its Gaussian nature, do not contribute in these estimators which remain unbiased. However, the presence of noise is felt in an increase in the scatter or covariance of these estimators which can be computed analytically:

$$\hat S_\ell^{A,B} = \sum_{\ell'} [\mathbf{M}^{-1}]_{\ell\ell'} \tilde S_{\ell'}^{A,B}; \quad \left\langle \delta\hat S_\ell^{A,B} \delta\hat S_{\ell'}^{A,B} \right\rangle = \sum_{LL'} \mathbf{M}^{-1}_{\ell L} \langle \delta\tilde S_L^{A,B} \delta\tilde S_{L'}^{A,B}\rangle \mathbf{M}^{-1}_{L'\ell'}; \quad \langle \hat S_\ell^{A,B}\rangle = S_\ell^{A,B}; \quad \{A, B\} \in \left\{\Psi, \Psi^2, (\nabla\Psi\cdot\nabla\Psi), \nabla^2\Psi\right\}. \tag{24}$$

Note that the mode-coupling matrix $\mathbf{M}$ is independent of the particular choice of the skew-spectrum. Hence, the same coupling matrix can be used to extract the power spectrum associated with the MFs, as the MFs are constructed from the linear combinations of generalized skew-spectra

$$[\hat{\mathcal{V}}_k^{(2)}]_\ell = \sum_{\ell'} [\mathbf{M}^{-1}]_{\ell\ell'} \left[\tilde{\mathcal{V}}_k^{(2)}\right]_{\ell'}; \qquad \left\langle \delta\hat{\mathcal{V}}_k^{(2)} \delta\hat{\mathcal{V}}_{k'}^{(2)} \right\rangle = \sum_{LL'} \mathbf{M}^{-1}_{\ell L} \left\langle \delta[\tilde{\mathcal{V}}_k^{(2)}]_\ell \delta[\tilde{\mathcal{V}}_{k'}^{(2)}]_{\ell'} \right\rangle \mathbf{M}^{-1}_{L'\ell'}. \tag{25}$$

The variance $\langle \delta S_\ell^{A,B} \delta S_\ell^{A,B}\rangle$ of various estimators can be constructed using the following procedure:

$$\langle \delta S_\ell^{A,B} \delta S_\ell^{A,B}\rangle = \frac{f_{\rm sky}^{-1}}{\Xi_\ell} \left[\mathcal{C}_\ell^{A,A}\mathcal{C}_\ell^{B,B} + [S_\ell^{A,B}]^2\right]; \tag{26}$$

$$\mathcal{C}_\ell^{\nabla\Psi\cdot\nabla\Psi,\nabla\Psi\cdot\nabla\Psi} = \sum_{\ell_1\ell_2}\ \Xi_\ell\ \mathcal{C}_{\ell_1}\mathcal{C}_{\ell_2}[\Pi_{\ell_1}+\Pi_{\ell_2}-\Pi_\ell]^2 J^2_{\ell_1\ell_2\ell}; \tag{27}$$

$$\mathcal{C}_\ell^{[\Psi^2,\Psi^2]} = \sum_{\ell_1\ell_2}\ \Xi_\ell\ \mathcal{C}_{\ell_1}\mathcal{C}_{\ell_2}J^2_{\ell_1\ell_2\ell}; \quad \mathcal{C}_\ell^{[\nabla^2\Psi,\nabla^2\Psi]} = \Pi_\ell^2\,\mathcal{C}_\ell; \quad \mathcal{C}_\ell^{\Phi,\Phi}\equiv\mathcal{C}_\ell. \tag{28}$$

We have used standard relations of 3*j* symbols, summarized in Appendix C, to derive these results. $\mathcal{C}_\ell^{A,A}$ denotes the power spectrum of a generic map $A(\hat{\Omega})$ that is used for the construction of generalized skew-spectra and $f_{\rm sky}$ is the fraction of sky coverage. The derivation depends on a Gaussian approximation, i.e. we ignore higher order NG in the fields. $\mathcal{C}_\ell$ is the ordinary CMB power spectra, including the effect of instrumental noise, $\mathcal{C}_\ell = \mathcal{C}_\ell^{\rm S}+\mathcal{C}_\ell^{\rm N}$. The first term represents cosmic variance and the second term is the effect of instrumental noise. For a survey with homogeneous noise, ignoring the effect of the beam we can write $\mathcal{C}_\ell^N = \Omega_{\rm p}\sigma_{\rm N}^2$ where $\Omega_{\rm p}$ is the pixel area and $\sigma_{\rm N}^2$ is the noise variance. In a noise-dominated regime, the MFs can be approximated by a Gaussian. The explicit expressions for the three skew-spectra that we have considered are as follows:

$$\left\langle[\delta S_\ell^{\Psi^2,\Psi}]^2\right\rangle = \frac{f_{\rm sky}^{-1}}{\Xi_\ell}\left[[S_\ell^{\Psi^2,\Psi}]^2+\mathcal{C}_\ell^{\Psi^2,\Psi^2}\mathcal{C}_\ell^{\Psi,\Psi}\right]; \tag{29}$$

$$\left\langle[\delta S_\ell^{\Psi^2,\nabla^2\Psi}]^2\right\rangle = \frac{f_{\rm sky}^{-1}}{\Xi_\ell}\left[[S_\ell^{\Psi^2,\nabla^2\Psi}]^2+\mathcal{C}_\ell^{\Psi^2,\Psi^2}\mathcal{C}_\ell^{\nabla^2\Psi,\nabla^2\Psi}\right]; \tag{30}$$

$$\left\langle[\delta S_\ell^{\nabla\Psi\cdot\nabla\Psi,\nabla^2\Psi}]^2\right\rangle = \frac{f_{\rm sky}^{-1}}{\Xi_\ell}\left[[S_\ell^{\nabla\Psi\cdot\nabla\Psi,\nabla^2\Psi}]^2+\mathcal{C}_\ell^{\nabla\Psi\cdot\nabla\Psi,\nabla\Psi\cdot\nabla\Psi}\mathcal{C}_\ell^{\nabla^2\Psi,\nabla^2\Psi}\right]. \tag{31}$$

The estimators for various skew-spectra are expected to be correlated to a certain extent. These can be expressed using following expression:

$$\langle\delta S_\ell^{A_1,B_1}\delta S_\ell^{A_2,B_2}\rangle = \frac{f_{\rm sky}^{-1}}{\Xi_\ell}\left[\mathcal{C}_\ell^{A_1,A_2}\mathcal{C}_\ell^{B_1,B_2}+S_\ell^{A_1,B_2}S_\ell^{A_2,B_1}\right]; \quad \{A_1,B_1,A_2,B_2\}\in\left\{\Psi,\Psi^2,(\nabla\Psi\cdot\nabla\Psi),\nabla^2\Psi\right\}. \tag{32}$$

The above results are sufficient to compute the lowest order corrections to MFs due to the presence of NG, as well as the scatter in the estimates in the presence of realistic mask and noise. The explicit expressions are as follows:

$$\left\langle\delta S_\ell^{\Psi^2,\Psi}\delta S_\ell^{\Psi^2,\nabla^2\Psi}\right\rangle = \frac{f_{\rm sky}^{-1}}{\Xi_\ell}\left[S_\ell^{\Psi^2,\Psi}S_\ell^{\Psi^2,\nabla^2\Psi}+\mathcal{C}_\ell^{\Psi^2,\Psi^2}\mathcal{C}_\ell^{\Psi,\nabla^2\Psi}\right]; \tag{33}$$

$$\left\langle\delta S_\ell^{\Psi^2,\Psi}\delta S_\ell^{\nabla\Psi\cdot\nabla\Psi,\nabla^2\Psi}\right\rangle = \frac{f_{\rm sky}^{-1}}{\Xi_\ell}\left[S_\ell^{\Psi^2,\nabla^2\Psi}S_\ell^{\Psi,\nabla\Psi\cdot\nabla\Psi}+\mathcal{C}_\ell^{\Psi^2,\nabla\Psi\cdot\nabla\Psi}\mathcal{C}_\ell^{\Psi,\nabla^2\Psi}\right]; \tag{34}$$

$$\left\langle\delta S_\ell^{\nabla\Psi\cdot\nabla\Psi,\nabla^2\Psi}\delta S_\ell^{\Psi^2,\nabla^2\Psi}\right\rangle = \frac{f_{\rm sky}^{-1}}{\Xi_\ell}\left[S_\ell^{\nabla\Psi\cdot\nabla\Psi,\nabla^2\Psi}S_\ell^{\Psi^2,\nabla^2\Psi}+\mathcal{C}_\ell^{\nabla\Psi\cdot\nabla\Psi,\Psi^2}\mathcal{C}_\ell^{\nabla^2\Psi,\nabla^2\Psi}\right]. \tag{35}$$

The additional cross-spectra that are introduced above are as follows:

$$\mathcal{C}_\ell^{\Psi,\nabla^2\Psi} = -\Pi_\ell\mathcal{C}_\ell; \qquad \mathcal{C}_\ell^{\Psi^2,\nabla\Psi\cdot\nabla\Psi} = 2\sum_{\ell_1\ell_2}\ \Xi_\ell\ \mathcal{C}_{\ell_1}\mathcal{C}_{\ell_2}[\Pi_{\ell_1}+\Pi_{\ell_2}-\Pi_\ell]J^2_{\ell_1\ell_2\ell}. \tag{36}$$

The signal-to-noise ratio (S/N) and the cross-correlation coefficients among various skew-spectra are defined as

$$\left(\frac{S}{N}\right)_\ell^{(i)} = \frac{S_\ell^{(i)}}{\langle[\delta S_\ell^{(i)}]^2\rangle^{1/2}}; \qquad r_\ell^{ij} = \frac{\langle\delta S_\ell^{(i)}\delta S_\ell^{(j)}\rangle}{\langle[\delta S_\ell^{(i)}]^2\rangle^{1/2}\langle[\delta S_\ell^{(j)}]^2\rangle^{1/2}}. \tag{37}$$

To compute the cross-correlation of skew-spectra $S_{{\rm I},\ell}^{A_1,B_1}$ and $S_{{\rm II},\ell}^{A_1,B_1}$, which source different bispectra $B_{{\rm I},\ell_1\ell_2\ell_3}$ and $B_{{\rm II},\ell_1\ell_2\ell_3}$ (either primary and secondary or two different models of primary bispectra) from the same data, we can use the following simple extension of equation (32):

$$\left\langle\delta S_{{\rm I},\ell}^{A_1,B_1}\delta S_{{\rm II},\ell}^{A_2,B_2}\right\rangle = \frac{f_{\rm sky}^{-1}}{\Xi_\ell}\left[\mathcal{C}_\ell^{A_1,A_2}\mathcal{C}_\ell^{B_1,B_2}+\sqrt{S_{{\rm I},\ell}^{A_1,B_2}S_{{\rm II},\ell}^{A_2,B_1}}\sqrt{S_{{\rm II},\ell}^{A_1,B_2}S_{{\rm I},\ell}^{A_2,B_1}}\right]; \quad \{A_1,B_1,A_2,B_2\}\in\left\{\Psi,\Psi^2,(\nabla\Psi\cdot\nabla\Psi),\nabla^2\Psi\right\}. \tag{38}$$

These results will be valid for near all-sky coverage and in a regime where noise dominates. Bias from inaccurate foreground subtraction is ignored. The results presented here can be extended to include estimation of kurt-spectra.The numerical results for the S/N for the local, equilateral, enfolded and orthogonal models are plotted in Figs 8–11, respectively. From these results, we find that in most cases the S/N is dominated by $\ell < 500$. Among the three skew-spectra we have considered $S_\ell^{(1)}$ achieves the maximum S/N due to optimum ℓ weighting. This is in agreement with our previous studies of MFs in weak lensing (Munshi et al. 2012b), tSZ (Munshi et al. 2012a) studies. Individual S_ℓs differ in their ℓ-dependent weightings of the bispectrum, with the weights for $S_\ell^{(1)}$ appearing to give the optimum balance among the three S_ℓ considered. The increase in S/N by changing experimental setup from *Planck* to EPIC is nominal as most of the signal is at low ℓ. We see that in order to reach S/N>3 would require $f_{\rm NL} > 20, 3\times10^3, 60, 10^3$ for the local, equilateral, orthogonal and enfolded models, respectively.

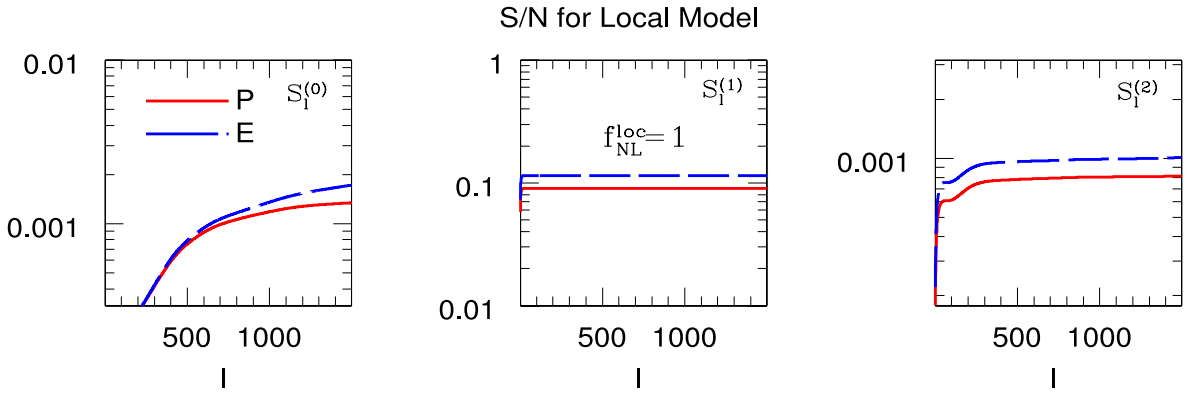

Figure 8. The cumulative S/N, $\sum_\ell (\mathrm{S/N})_\ell^{\mathrm{loc}}$, for various skew-spectra that correspond to the *local* model of primordial NG. These results correspond to $f_{\mathrm{NL}}^{\mathrm{loc}} = 1$. Each panel shows results for *Planck* (143 GHz channel) and for EPIC (150 GHz channel). The left, middle and right panels correspond to $S_\ell^{(0)}$, $S_\ell^{(1)}$ and $S_\ell^{(2)}$, respectively. The expressions for the covariances are listed in equations (29)–(31). We have assumed a full sky coverage $f_{\mathrm{sky}} = 1$ for both of these experiments.

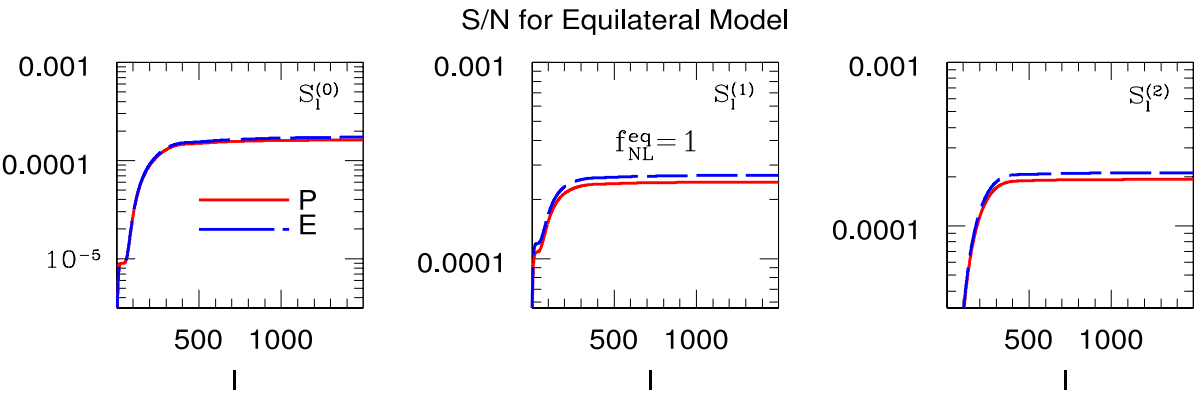

Figure 9. Same as previous figure but for the *equilateral* model ($f_{\mathrm{NL}}^{\mathrm{eq}} = 1$) of primordial NG.

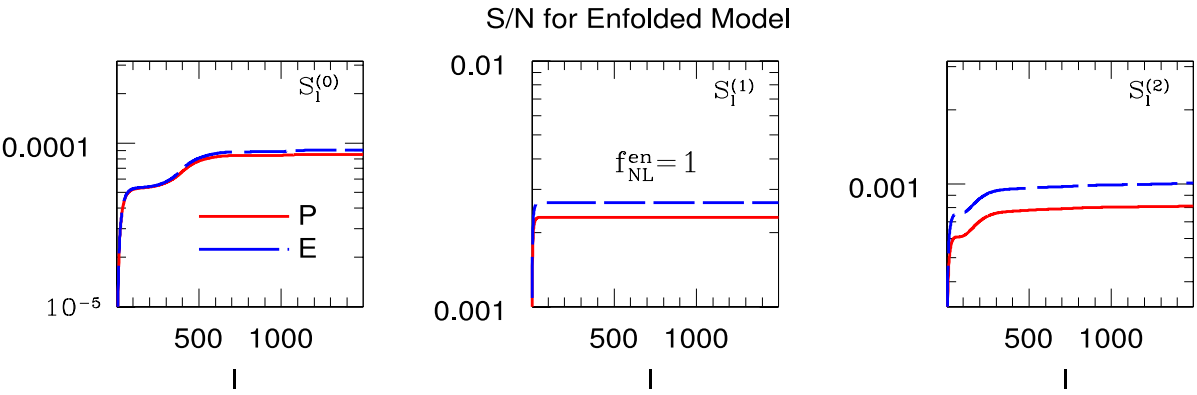

Figure 10. Same as previous figure but for the *enfolded* model ($f_{\mathrm{NL}}^{\mathrm{en}} = 1$) of primordial NG.

5 MODAL DECOMPOSITION AND RECONSTRUCTING MFs

In recent years, modal decomposition of a generic bispectrum, in terms of a separable or orthogonal basis, has been proposed (e.g. Fergusson, Liguori & Shellard 2010a). 3D modes $\mathcal{Q}_n^{\ell_1\ell_2\ell_3}(x)$ (to be defined later) are constructed from one-dimensional modes $q_p^\ell(x)$, and the coefficients in the expansion can then be used to reconstruct the bispectrum or trispectrum. The primary aim of this section is to express the skewness-spectra introduced in the text in terms of the coefficients characterizing the modal expansion of the bi- and trispectrum.

Following the procedure detailed in Fergusson et al. (2010a), we introduce the following modal decomposition of the reduced bispectrum $b_{\ell_1\ell_2\ell_3}$ in terms of modal function denoted as $\mathcal{Q}_n^{\ell_1\ell_2\ell_3}(x)$:

$$q_p^\ell(x) = \frac{2}{\pi}\int \mathrm{d}k\; q_p(k)\;\Delta_\ell(k)\;j_\ell(kx); \qquad \mathcal{Q}_n^{\ell_1\ell_2\ell_3}(x) \equiv q_{\{p}^{\ell_1}(x) q_q^{\ell_2}(x) q_{r\}}^{\ell_3}(x); \tag{39}$$

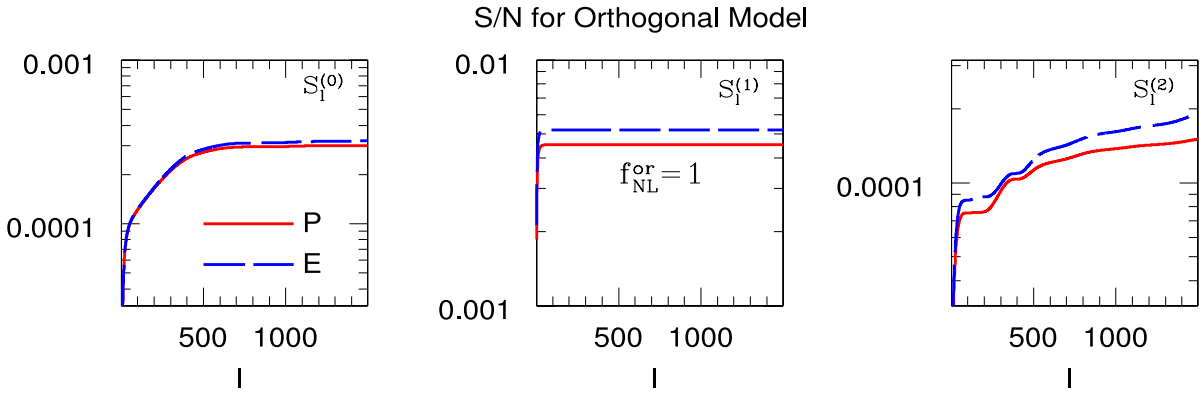

Figure 11. Same as previous figure but for the *orthogonal* model ($f_{\rm NL}^{\rm orth} = 1$) of primordial NG.

$$b_{\ell_1\ell_2\ell_3} \equiv \Delta_\Phi^2 f_{\rm NL} \sum_n \alpha_n^{\mathcal{Q}} \int x^2 {\rm d}x \; \mathcal{Q}_n^{\ell_1\ell_2\ell_3}(x). \tag{40}$$

The separable basis functions q_p^ℓ are convolutions of the spatial basis functions $q_p(k)$ and the transfer function $\Delta_\ell(k)$. They reduce the dimensionality of the integral by expressing the 3D integral in terms of three one-dimensional integrals that are easy to evaluate. The 3D basis functions $\mathcal{Q}_n^{\ell_1\ell_2\ell_3}(x)$ are then constructed from the one-dimensional $q_p^\ell(x)$ basis functions. The curly brackets in $q_{\{p}^{\ell_1}(x) q_q^{\ell_2}(x) q_{r\}}^{\ell_3}(x)$ represents all possible permutations of the indices $\ell_1\ell_2\ell_3$. The index n represents a specific combination of one-dimensional modes described by the triplets of indices$\{pqr\}$; a mapping between the two is implicitly assumed $n \leftrightarrow \{pqr\}$ below.

The speed and accuracy of the modal decomposition depends ultimately on the smoothness of the reduced bispectrum. The modal decomposition above was carried out on separable basis functions $q_p^\ell(x)$. Nevertheless, the Gram–Schmidt orthogonalization procedure can be employed to construct a set of orthogonal modes in which an equivalent analysis can be formulated. Completeness of the orthonormal basis is important for the accuracy of the modal decomposition. The bispectrum is expanded in a finite set of modes:

$$\frac{v_{\ell_1} v_{\ell_2} v_{\ell_3}}{\sqrt{\mathcal{C}_{\ell_1}\mathcal{C}_{\ell_2}\mathcal{C}_{\ell_3}}} b_{\ell_1\ell_2\ell_3} = \sum_{n\leftrightarrow\{pqr\}} \alpha_n^{\mathcal{Q}} \mathcal{Q}_n; \tag{41}$$

$$M_p(\hat{\Omega}) = \sum_{lm} q_p^\ell(x) \frac{\Psi_{\ell m}}{v_\ell \sqrt{\mathcal{C}_\ell}} Y_{\ell m}(\hat{\Omega}); \qquad M_n(\hat{\Omega}) = M_p(\hat{\Omega}) M_r(\hat{\Omega}) M_s(\hat{\Omega}). \tag{42}$$

Here, $M_p(\hat{\Omega})$ are filtered maps constructed from the harmonics $\Psi_{\ell m}$ of the original map Ψ. The functions $v_\ell = (2\ell+1)^{1/6}$ are introduced to remove any residual ℓ-dependence in the reduced bispectrum $b_{\ell_1\ell_2\ell_3}$. We also define

$$\left\langle \beta_n^{\mathcal{Q}} \right\rangle \equiv \int {\rm d}\hat{\Omega} \int x^2 {\rm d}x \; \langle M_n(\hat{\Omega}) \rangle = \sum_{n'} \Gamma_{nn'} \alpha_{n'}^{\mathcal{Q}}; \qquad \hat{\alpha}_n^{\mathcal{Q}} = \sum_n [\Gamma^{-1}]_{nn'} \beta_{n'}^{\mathcal{Q}}; \qquad \Gamma_{nn'} = \sum_{\ell_1\ell_2\ell_3} \frac{w_{\ell_1\ell_2\ell_3}}{v_{\ell_1}^2 v_{\ell_2}^2 v_{\ell_3}^2} \mathcal{Q}_n \mathcal{Q}_{n'}. \tag{43}$$

Next, the triplets of skew-spectra $S_\ell^{(0)}$, $S_\ell^{(1)}$, $S_\ell^{(2)}$ can be constructed from the modal coefficients $\alpha_n^{\mathcal{Q}}$:

$$3\sigma_0^4 \; \hat{S}_\ell^{(0)} \equiv \sum_{\ell_1\ell_2} I_{\ell_1\ell_2\ell}^2 b_{\ell_1\ell_2\ell} = \Delta_\Phi^2 f_{\rm NL} \sum_n \sum_{\ell_1\ell_2} \hat{\alpha}_n^{\mathcal{Q}} \int x^2 {\rm d}x \;\; \mathcal{Q}_n^{\ell_1\ell_2\ell}(x); \tag{44}$$

$$4\sigma_0^2\sigma_1^2 \; \hat{S}_\ell^{(1)} \equiv \sum_{\ell_1\ell_2} I_{\ell_1\ell_2\ell}^2 (\Pi_{\ell_1} + \Pi_{\ell_2} + \Pi_{\ell_3}) b_{\ell_1\ell_2\ell} = \Delta_\Phi^2 f_{\rm NL} \sum_n \sum_{\ell_1\ell_2} \hat{\alpha}_n^{\mathcal{Q}} \; (\Pi_{\ell_1} + \Pi_{\ell_2} + \Pi_\ell) \int x^2 {\rm d}x \;\; \mathcal{Q}_n^{\ell_1\ell_2\ell}(x); \tag{45}$$

$$\begin{aligned} 2\sigma_1^4 \; \hat{S}_\ell^{(2)} &\equiv \sum_{\ell_1\ell_2} I_{\ell_1\ell_2\ell}^2 [(\Pi_{\ell_1} + \Pi_{\ell_2} - \Pi_\ell)\Pi_\ell + {\rm cyc.perm.}] b_{\ell_1\ell_2\ell} \\ &= \Delta_\Phi^2 f_{\rm NL} \sum_n \sum_{\ell_1\ell_2} \hat{\alpha}_n^{\mathcal{Q}} [(\Pi_{\ell_1} + \Pi_{\ell_2} - \Pi_\ell)\Pi_\ell + {\rm cyc.perm.}] \int x^2 {\rm d}x \, \mathcal{Q}_n^{\ell_1\ell_2\ell}(x). \end{aligned} \tag{46}$$

We have suppressed the experimental beams in these expressions for clarity.

Similar expressions for modal decomposition of the (reduced) trispectrum can be found in Regan, Shellard & Fergusson (2010). The modal expansion of the trispectrum $\tau_{\ell_3\ell_3}^{\ell_1\ell_2}(\ell)$ requires a five-dimensional basis and the coefficients of expansion can be used to reconstruct the MFs

$$\tau_{\ell_3\ell_4}^{\ell_1\ell_2}(\ell) \propto \Delta_\phi^3 \sum_m \alpha_m^{\mathcal{Q}} \int x_1^2 {\rm d}x_1 x_2^2 {\rm d}x_2 \mathcal{Q}_{\ell_1\ell_2\ell_3\ell_4\ell}(x_1, x_2); \quad \mathcal{Q}_{\ell_1\ell_2\ell_3\ell_4\ell}(x_1, x_2) = q_p^{\ell_1}(x_1) q_r^{\ell_2}(x_1) q_s^{\ell_3}(x_2) q_u^{\ell_4}(x_2) r_v^\ell(x_1, x_2); \tag{47}$$

$$r_v^{\ell}(x_1, x_2) = \frac{2}{\pi} \int \mathrm{d}k\, k\, r_v(k)\, j_\ell(kx_1)\, j_\ell(kx_2). \tag{48}$$

These expressions are useful for the construction of an estimator for τ from a CMB map which can then be used in equations (B10)–(B13) for estimation of kurt-spectra associated with MFs. This will provide a consistency check for the results obtained using direct estimators of MFs defined in equations (B14)–(B15).

The actual data analysis pipelines for MF analysis and that of 3D modal decomposition are very different. Relating perturbative expansion of MFs and using the modal decomposition to reconstruct the MFs at intermediate steps may lead to a better understanding of the systematics affecting their estimation.

6 ODD-PARITY BISPECTRUM AND MFs

Most analyses of the bispectrum assume the bispectrum to be of even parity. Recently, the possibility of odd-parity bispectrum was underlined by Kamionkowski & Souradeep (2011). Such a bispectrum *cannot* arise from projecting the 3D density perturbations. Nevertheless, the odd-parity bispectrum can result from lensing of the CMB by a chiral gravitational wave background or from cosmological birefringence (Komatsu et al. 2001; Feng et al. 2006; Wu et al. 2009). Models with a time-dependent quintessence field that couples to pseudo-scalar of the electromagnetic field and induced rotation of linear polarization and generate magnetic 'B' mode polarization from pure electric 'E' mode and hence induce an odd-parity mixed temperature-polarization bispectra (Caroll, Field & Jackiw 1990; Lue, Wang & Kamionkowski 1990; Caroll 1998).

The reduced bispectrum $b_{\ell_1\ell_2\ell_3}$ introduced in the equation (13) is replaced by the following equation:

$$\langle a_{\ell_1 m_1} a_{\ell_2 m_2} a_{\ell_3 m_3}\rangle = B_{\ell_1\ell_2\ell_3} \begin{pmatrix} \ell_1 & \ell_2 & \ell_3 \\ m_1 & m_2 & m_3 \end{pmatrix}; \quad B_{\ell_1\ell_2\ell_3} = \mathcal{I}_{\ell_1\ell_2\ell_3} b_{\ell_1\ell_2\ell_3}; \tag{49}$$

$$\mathcal{I}_{\ell_1\ell_2\ell_3} = \frac{\Pi_{\ell_2}\Pi_{\ell_3}}{\Pi_{\ell_1} - \Pi_{\ell_2} - \Pi_{\ell_3}} \sqrt{\frac{\Xi_{\ell_1}\Xi_{\ell_2}\Xi_{\ell_3}}{4\pi}} \begin{pmatrix} \ell_1 & \ell_2 & \ell_3 \\ 0 & -1 & 1 \end{pmatrix}. \tag{50}$$

It can be shown that $\mathcal{I}_{\ell_1\ell_2\ell_3} = I_{\ell_1\ell_2\ell_3}$ for even parity, i.e. $\ell_1 + \ell_2 + \ell_3 =$ even, but it remains non-zero also for odd parity, i.e. $\ell_1 + \ell_2 + \ell_3 =$ odd,

$$S_\ell^{(0)} = \frac{2}{3\sigma_0^4}\, \frac{1}{\Xi_\ell} \sum_{\ell_1 > \ell_2} b_{\ell_1\ell_2\ell}\, \mathcal{I}^2_{\ell_1\ell_2\ell}\, b_{\ell_1}\, b_{\ell_2}\, b_\ell; \tag{51}$$

$$S_\ell^{(1)} = \frac{1}{2\sigma_0^2\sigma_1^2}\, \frac{1}{\Xi_\ell} \sum_{\ell_1 > \ell_2} (\Pi_{\ell_1} + \Pi_{\ell_2} + \Pi_\ell)\, b_{\ell_1\ell_2\ell}\, \mathcal{I}^2_{\ell_1\ell_2\ell}\, b_{\ell_1}\, b_{\ell_2}\, b_\ell; \tag{52}$$

$$S_\ell^{(2)} = \frac{1}{\sigma_1^4}\, \frac{1}{\Xi_\ell} \sum_{\ell_1 > \ell_2} [(\Pi_\ell + \Pi_{\ell_1} - \Pi_{\ell_2})\Pi_{\ell_2} + \text{cyc.perm.}]\, b_{\ell_1\ell_2\ell}\, \mathcal{I}^2_{\ell_1\ell_2\ell}\, b_{\ell_1}\, b_{\ell_2}\, b_\ell. \tag{53}$$

The summations over possible modes defined by (ℓ, ℓ_1, ℓ_2) are restricted to $\ell + \ell_1 + \ell_2 =$ odd (o). Note that the definition of reduced bispectrum given in equation (13) enforces $\ell + \ell_1 + \ell_2 =$ even (e), i.e. includes only even-parity modes. These results can be generalized to the case of kurt-spectra.

Clearly there is no obvious source that is expected to reach the S/N of detectability. However, such null-tests for odd-parity skew-spectra can definitely be included to check for possible contamination from systematics, or as tests for as-yet unknown new physics.

The odd- and even-parity *optimized* skew-spectra can likewise be expressed as

$$S_\ell^{(\mathrm{o})} = \sum_{\ell_1 \geq \ell_2} \frac{\hat{B}_{\ell_1\ell_2\ell} B_{\ell_1\ell_2\ell}}{\mathcal{C}_{\ell_1}\mathcal{C}_{\ell_2}\mathcal{C}_\ell}; \quad \ell + \ell_1 + \ell_2 = \text{odd}; \tag{54}$$

$$S_\ell^{(\mathrm{e})} = \sum_{\ell_1 \geq \ell_2} \frac{\hat{B}_{\ell_1\ell_2\ell} B_{\ell_1\ell_2\ell}}{\mathcal{C}_{\ell_1}\mathcal{C}_{\ell_2}\mathcal{C}_\ell}; \qquad \ell + \ell_1 + \ell_2 = \text{even}. \tag{55}$$

In the first case, only odd modes are included while in the second case we restrict to even modes, thus reducing it to the usual skew-spectrum described in Munshi & Heavens (2010). If we further assume that the even and odd-parity contributions can be separated with respective amplitudes given by $f_{\mathrm{NL}}^{(\mathrm{e})}$ and $f_{\mathrm{NL}}^{(\mathrm{o})}$ for a specific model of NG, we can write

$$B_{\ell_1\ell_2\ell_3} = f_{\mathrm{NL}}^{(\mathrm{e})} B^{(\mathrm{e})}_{\ell_1\ell_2\ell_3} + f_{\mathrm{NL}}^{(\mathrm{o})} B^{(\mathrm{o})}_{\ell_1\ell_2\ell_3}. \tag{56}$$

The estimators for $f_{NL}^{(\rm e)}$ and $f_{NL}^{(\rm o)}$ are given by

$$f_{NL}^{(\rm e)/(\rm o)} = \frac{1}{\rm N^{(e)/(o)}} \sum_{\ell_1 \geq \ell_2 \geq \ell_3} \frac{\hat{B}_{\ell_1\ell_2\ell_3} B_{\ell_1\ell_2\ell_3}}{\mathcal{C}_{\ell_1}\mathcal{C}_{\ell_2}\mathcal{C}_{\ell_3}}; \quad \ell + \ell_1 + \ell_2 = \text{even/odd}; \qquad \rm N^{(e)/(o)} = \sum_{\ell_1 \geq \ell_2 \geq \ell_3} \frac{\hat{B}_{\ell_1\ell_2\ell_3} B^{(e)/(o)}_{\ell_1\ell_2\ell_3}}{\mathcal{C}_{\ell_1}\mathcal{C}_{\ell_2}\mathcal{C}_{\ell_3}}. \tag{57}$$

The generalization to include partial sky coverage and to handle the inhomogeneous noise can be done following the prescription in Munshi & Heavens (2010).

Generalization to the case of odd-parity kurt-spectra can be done in a similar manner. We start by noting that all-sky pairing function $P^{\ell_1\ell_2}_{\ell_3\ell_4}(\ell)$ and the flat-sky version p can be linked by the following expression: $P^{\ell_1\ell_2}_{\ell_3\ell_4}(\ell) = I_{\ell_1\ell_2\ell} I_{\ell_3\ell_4\ell}\ \ p^{\ell_1\ell_2}_{\ell_3\ell_4}(\ell)$. Using equation (50), we modify this expression as: $P^{\ell_1\ell_2}_{\ell_3\ell_4}(\ell) = \mathcal{I}_{\ell_1\ell_2\ell}\mathcal{I}_{\ell_3\ell_4\ell}\ \ p^{\ell_1\ell_2}_{\ell_3\ell_4}(\ell)$. Using this modified $P^{\ell_1\ell_2}_{\ell_3\ell_4}(\ell)$ and other terms that are obtained by permutations of indices, e.g. $P^{\ell_1\ell_3}_{\ell_2\ell_4}(\ell)$ and $P^{\ell_1\ell_4}_{\ell_2\ell_3}(\ell)$, one can finally construct the $[T^{(i)}]^{\ell_1\ell_2}_{\ell_3\ell_4}(\ell)$ that will match with the ordinary trispectrum when $\Sigma_U =$ even and $\Sigma_L =$ even condition is satisfied but will not be vanishing when one of these conditions is violated. The total trispectrum can be constructed from four different contributions:

$$[T^{(i)}]^{\ell_1\ell_2}_{\ell_3\ell_4}(\ell) = \alpha\ [T^{(\rm e-e),(i)}]^{\ell_1\ell_2}_{\ell_3\ell_4}(\ell) + \beta\ [T^{(\rm o-e),(i)}]^{\ell_1\ell_2}_{\ell_3\ell_4}(\ell) + \gamma\ [T^{(\rm o-e),(i)}]^{\ell_1\ell_2}_{\ell_3\ell_4}(\ell) + \delta\ [T^{(\rm o-o),(i)}]^{\ell_1\ell_2}_{\ell_3\ell_4}(\ell). \tag{58}$$

Here, $(\alpha, \beta, \gamma, \delta)$ define the relative contributions from four different types of trispectra. We can now define the odd-parity kurt-spectra:

$$K^{(i)}_\ell = \sum_{\ell_1 \geq \ell_2 \geq \ell_3 \geq \ell_4} \frac{1}{\Xi_\ell} [T^{(i)}]^{\ell_1\ell_2}_{\ell_3\ell_4}(\ell) \mathcal{J}_{\ell_1\ell_2\ell}\mathcal{J}_{\ell_3\ell_4\ell}; \qquad \mathcal{J}_{\ell_1\ell_2\ell} = \frac{\mathcal{I}_{\ell_1\ell_2\ell}}{\Xi_\ell}. \tag{59}$$

Depending on whether $\Sigma_U = \ell_1 + \ell_2 + \ell$ and $\Sigma_L = \ell_3 + \ell_4 + \ell$ are restricted to even (e) or odd (o) we have four different possible combinations, i.e. $[K^{(i)}_\ell]^{(\rm o-o)}$ when Σ_U and Σ_L are both odd and similarly one can have $[K^{(i)}_\ell]^{(\rm o-e)}$ and $[K^{(i)}_\ell]^{(\rm e-o)}$ or $[K^{(i)}_\ell]^{(\rm e-e)}$ for other possible choices. The estimator $[K^{(i)}_\ell]^{(\rm e-e)}$ denotes the usual choice in the literature. The modifications of the optimized kurt-spectra defined in Munshi et al. (2011a) can be done using the same techniques e.g. using suitably defined optimized kurt-spectra associated with the odd–odd parity trispectra we have the following estimators for the amplitude δ:

$$\delta = \frac{1}{N^{(\rm o-o)}} \sum_{\ell_1 \geq \ell_2 \geq \ell_3 \geq \ell_4} \frac{1}{\Xi_\ell} \frac{\hat{T}^{\ell_1\ell_2}_{\ell_3\ell_4}(\ell) T^{\ell_1\ell_2}_{\ell_3\ell_4}(\ell)}{\mathcal{C}_{\ell_1}\mathcal{C}_{\ell_2}\mathcal{C}_{\ell_3}\mathcal{C}_{\ell_4}}; \qquad \Sigma_U = \text{odd}, \Sigma_L = \text{odd}; \qquad N^\delta = \sum_{\ell_1 \geq \ell_2 \geq \ell_3 \geq \ell_4} \frac{1}{\Xi_\ell} \frac{\hat{T}^{\ell_1\ell_2}_{\ell_3\ell_4}(\ell) T^{\ell_1\ell_2}_{\ell_3\ell_4}(\ell)}{\mathcal{C}_{\ell_1}\mathcal{C}_{\ell_2}\mathcal{C}_{\ell_3}\mathcal{C}_{\ell_4}}. \tag{60}$$

In the above expression, we have restricted both the triplets defined by Σ_U and Σ_L to odd-parity modes. The normalization N^δ is also defined using the same restrictions. The estimators for α, β and γ can also be constructed in an analogous manner.

7 MFs IN A NEEDLET BASIS

The use of wavelets in the CMB is now well established (Freeden & Schneider 1998; Antoine & Vandergheynst 1999; McEwen, Hobson & Lasenby 2006; McEwen et al. 2007). Wavelet analysis provides an intermediate choice between real-space analysis and analysis in the harmonic domain and is particularly suitable for localized signals. Needlets are special types of spherical wavelets that allow localized filtering in both real space and in the harmonic domain. They have compact support in the harmonic domain but are still very well localized in the pixel basis (Narcowich, Peterushev & Ward 2006; Guilloux, Fay & Cardoso 2007; Marinucci et al. 2008). It has been used previously for foreground subtraction (Hansen et al. 2006), component separation (Starck et al. 2006; Basak & Delabrouille 2012), point source detection (Sanz et al. 2006) polarization analysis (Cabella, Natoli & Silk 2007) as well as testing NG (Cabella et al. 2004; Vielva et al. 2004; Rudjord et al. 2009; Donzelli et al. 2012) and detection of features in the CMB sky (Pietrobon et al. 2008). We start with the decomposition of a generic function $\Psi(\hat{\Omega})$ using a needlet basis $\Phi_{jk}(\hat{\Omega})$

$$\Psi(\hat{\Omega}) = \sum_{jk} \Psi_{jk}\, \Phi_{jk}(\hat{\Omega}); \qquad \Phi_{jk}(\hat{\Omega}) = \sqrt{\lambda_{jk}} \sum_\ell \varpi^{(j)}_\ell \sum_{m=-\ell}^{\ell} Y^*_{\ell m}(\hat{\Omega}) Y_{\ell m}(\hat{\Omega}_{jk}); \qquad \varpi^{(j)}_\ell = \varpi\left(\frac{\ell}{\mathcal{B}^j}\right). \tag{61}$$

Here, $\{\hat{\Omega}_{jk}\}$ defines a set of *cubature points* on the unit sphere corresponding to frequency j, and $\{\lambda_{jk}\}$ denotes the *cubature weights*. The needlet coefficients $\{\lambda_{jk}\}$ are proportional to the pixel area. For a given HEALPIX[9] resolution, the centres of pixels can serve as cubature points and $\lambda_{jk} = (4\pi/N^j_{\rm pix})$ where $N^j_{\rm pix}$ is the total number of pixels at a given resolution. The *weight function or filter* $\varpi(t)$ satisfies three different conditions. *Compact support*: $\varpi(t)$ is strictly positive in the interval $t \in [\mathcal{B}^{-1}, \mathcal{B}]$ for a given 'dilation parameter' $\mathcal{B}$, thus $\varpi^{(j)}_\ell$ has support in $\ell \in [\mathcal{B}^{j-1}, \mathcal{B}^{j+1}]$. *Smoothness*: $\varpi(t)$ is infinitely differentiable in $(0,\infty)$, and finally, *partition of unity*: for any given ℓ, we have $\sum_j [\varpi^{(j)}_\ell]^2 = 1$ for all $\ell > \mathcal{B}$. The specific recipe for constructing $\varpi^{(j)}_\ell$ can be found in Marinucci et al. (2008). The needlet coefficients Ψ_{jk} are given by the inverse needlet transform and are expressed in terms of the harmonic coefficents $\Psi_{\ell m}$ of the map $\Psi(\hat{\Omega})$:

$$\Psi_{jk} \equiv \int {\rm d}\hat{\Omega}\ \Phi_{jk}(\hat{\Omega})\Psi(\hat{\Omega}) = \sqrt{\lambda_{jk}} \sum_\ell \varpi^{(j)}_\ell \sum_{m=-\ell}^{\ell} \Psi_{\ell m} b_\ell\ Y_{\ell m}(\hat{\Omega}_{jk}). \tag{62}$$

[9] http://healpix.jpl.nasa.gov

The above expression relates the needlet coefficients Ψ_{jk} to the harmonic coefficients $\Psi_{\ell m}$. The power spectrum $\mathcal{C}_\ell$ and the *needlet power spectrum* $\beta_j^{(1,1)}$ are related through the following expression:

$$\beta_j^{(\Psi,\Psi)} \equiv \frac{1}{N_{\rm pix}^{(j)}} \sum_k \Psi_{jk}\Psi^*_{jk} = \sum_\ell [\varpi_\ell^{(j)}]^2 \frac{\Xi_\ell}{4\pi}\mathcal{C}_\ell b_l^2; \qquad \sum_j \beta_j^{(\Psi,\Psi)} = \sum_\ell \frac{\Xi_\ell}{4\pi}\mathcal{C}_\ell b_\ell^2 = \langle [\delta\Psi(\hat{\Omega})]^2\rangle. \tag{63}$$

Thus, the needlet power spectrum is simply the variance computed using a specific set of *filters* $\varpi_j^{(\ell)}$. The needlet power spectrum computed with partial sky coverage can likewise be expressed in terms of the harmonic power spectrum obtained from the partial sky coverage:

$$\tilde{\beta}_j^{(\Psi,\Psi)} \equiv \frac{1}{N_{\rm pix}^{(j)}} \sum_k \tilde{\Psi}_{jk}\tilde{\Psi}^*_{jk} = \sum_\ell [\varpi_\ell^{(j)}]^2 \frac{\Xi_\ell}{4\pi}\tilde{\mathcal{C}}_\ell b_\ell^2. \tag{64}$$

The convolved power spectrum recovered from the partial sky $\tilde{\mathcal{C}}_\ell$ can be expressed in terms of the all-sky power spectrum $\tilde{\mathcal{C}}_\ell = \mathbf{M}_{\ell\ell'}\mathcal{C}_{\ell'}$ ($\mathbf{M}_{\ell\ell'}$ is defined in equation 23). It is possible to express the needlet power spectrum $\tilde{\beta}_j$ from the partial sky in terms of the all-sky power spectra $\tilde{\beta}_j$ which allows definition of an unbiased estimator

$$\tilde{\beta}_j = \sum_{j'} \mathbb{T}_{jj'}\beta_j; \qquad \hat{\beta}_j = \sum_{j'} \mathbb{T}^{-1}_{jj'}\tilde{\beta}_{j'}, \tag{65}$$

where we define

$$\mathbb{T}_{jj'} = \sum_{\ell'} \mathbb{K}_{j\ell'}\mathbb{S}^{-1}_{\ell' j'}; \qquad \mathbb{K}_{\ell' j} = \sum_\ell [\varpi_\ell^{(j)}]^2(2\ell+1)\mathbf{M}_{\ell\ell'}; \qquad \mathbb{S}_{\ell j} = (2\ell+1)[\varpi_\ell^{(j)}]^2. \tag{66}$$

A similar construction $\beta_j^{(\Psi,\Psi')}$ involving two different fields Ψ and Ψ' is possible which will depend on the cross-spectra involving these two fields $\langle \Psi_{\ell m}\Psi'_{\ell m}\rangle = \mathcal{C}_\ell^{\Psi\Psi'}\delta_{\ell\ell'}\delta_{mm'}$. Such *needlet cross-spectra* have already been used in cross-correlating large-scale tracers such as the maps of galaxy distributions from the surveys such as NVSS and CMB maps from *WMAP* to study the ISW effect (Petroboni, Balbi & Marinucci 2006).

The *needlet bispectrum* $S_{j_1 j_2 j_3}$ and *trispectrum* can similarly be expressed in terms of the bispectrum $B_{\ell_1\ell_2\ell_3}$ and trispectrum using the following expressions:

$$S_{j_1 j_2 j_3} = \frac{1}{N_{\rm pix}^{(j)}} \sum_k \Psi_{j_1 k}\Psi_{j_2 k}\Psi_{j_3 k} = \sum_{\ell_1\ell_2\ell_3} \varpi_{\ell_1}^{(j_1)}\varpi_{\ell_2}^{(j_2)}\varpi_{\ell_3}^{(j_3)} I_{\ell_1\ell_2\ell_3} B_{\ell_1\ell_2\ell_3} b_{\ell_1} b_{\ell_2} b_{\ell_3}; \tag{67}$$

$$T_{j_1 j_2 j_3 j_4} = \frac{1}{N_{\rm pix}^{(j)}} \sum_k \Psi_{j_1 k}\Psi_{j_2 k}\Psi_{j_3 k}\Psi_{j_4 k} = \sum_{\ell_1\ell_2\ell_3} \varpi_{\ell_1}^{(j_1)}\varpi_{\ell_2}^{(j_2)}\varpi_{\ell_3}^{(j_3)}\varpi_{\ell_4}^{(j_4)} \sum_\ell \frac{1}{\Xi_\ell} I_{\ell_1\ell_2\ell} I_{\ell_3\ell_4\ell} T^{\ell_1\ell_2}_{\ell_3\ell_4}(\ell) b_{\ell_1} b_{\ell_2} b_{\ell_3} b_{\ell_4}. \tag{68}$$

Thus, the needlet bispectrum or trispectrum is equivalent to the ordinary skewness or kurtosis with varying weights specified by the indices $\{j_i\}$. Note that individual estimates of the needlet bispectrum $S_{j_1 j_2 j_3}$ are expected to be noise dominated.

Next, we introduce here the concept of the skew-spectra in the needlet domain. We expand the maps Ψ^2, $\nabla^2\Psi$ and $\nabla\Psi\cdot\nabla\Psi$ in their needlet basis:

$$\begin{aligned}
[\Psi^2]_{jk} &= \int {\rm d}\hat{\Omega}\ \Phi_{jk}(\hat{\Omega})[\Psi^2(\hat{\Omega})] = \int {\rm d}\hat{\Omega}\ \Phi_{jk}(\hat{\Omega}) \sum_{j_1 k_1} \Psi_{j_1 k_1}\Phi_{j_1 k_1}(\hat{\Omega}) \sum_{j_2 k_2} \Psi_{j_2 k_2}\Phi_{j_2 k_2}(\hat{\Omega}) \\
&= \sum_{j_1 k_1}\sum_{j_2 k_2} \Psi_{j_1 k_1}\Psi_{j_2 k_2}\sqrt{\lambda_{jk}}\sqrt{\lambda_{j_1 k_1}}\sqrt{\lambda_{j_2 k_2}} \sum_{\ell_1\ell_2} \varpi_\ell^{(j)}\varpi_{\ell_1}^{(j_1)}\varpi_{\ell_2}^{(j_2)} I_{\ell_1\ell_2\ell} \\
&\quad \times \sum_{m m_1 m_2} \begin{pmatrix} \ell_1 & \ell_2 & \ell \\ m_1 & m_2 & m \end{pmatrix} Y_{\ell_1 m_1}(\hat{\Omega}_{j_1 k_1}) Y_{\ell_2 m_2}(\hat{\Omega}_{j_2 k_2}) Y_{\ell m}(\hat{\Omega}_{jk}); \qquad (69) \\
[\nabla^2\Phi]_{jk} &= \int {\rm d}\hat{\Omega}\ \Phi_{jk}(\hat{\Omega})[\nabla^2\Psi(\hat{\Omega})] = -\sqrt{\lambda_{jk}} \sum_\ell \varpi_\ell^{(j)}\Pi_\ell b_\ell \sum_{m=-\ell}^{\ell} \Psi_{\ell m} Y_{\ell m}(\hat{\Omega}_{jk}); \\
[\nabla\Psi\cdot\nabla\Psi]_{jk} &= \int {\rm d}\hat{\Omega}\ \Phi_{jk}(\hat{\Omega})[\nabla\Psi(\hat{\Omega})\cdot\nabla\Psi(\hat{\Omega})] = \int {\rm d}\hat{\Omega}\ \Phi_{jk}(\hat{\Omega}) \sum_{j_1 k_1} \Psi_{j_1 k_1}\nabla\Phi_{j_1 k_1}(\hat{\Omega}) \cdot \sum_{j_2 k_2} \Psi_{j_2 k_2}\nabla\Phi_{j_2 k_2}(\hat{\Omega}) \qquad (70) \\
&= \frac{1}{3}\sum_{j_1 k_1}\sum_{j_2 k_2} \Psi_{j_1 k_1}\Psi_{j_2 k_2}\sqrt{\lambda_{jk}}\sqrt{\lambda_{j_1 k_1}}\sqrt{\lambda_{j_2 k_2}} \sum_{\ell_1\ell_2} \varpi_\ell^{(j)}\varpi_{\ell_1}^{(j_1)}\varpi_{\ell_2}^{(j_2)} (\Pi_{\ell_1} + \Pi_{\ell_2} - \Pi_\ell) I_{\ell_1\ell_2\ell} \\
&\quad \times \sum_{m m_1 m_2} (-1)^m \begin{pmatrix} \ell_1 & \ell_2 & \ell \\ m_1 & m_2 & m \end{pmatrix} Y_{\ell_1 m_1}(\hat{\Omega}_{j_1 k_1}) Y_{\ell_2 m_2}(\hat{\Omega}_{j_2 k_2}) Y_{\ell m}(\hat{\Omega}_{jk}). \qquad (71)
\end{aligned}$$

We now define the skew-spectra, labelled by j, in the needlet basis by the following expressions:

$$\beta_j^{(\Psi^2,\Psi)} = \frac{1}{N_{\rm pix}^{(j)}}\sum_k [\Psi^2]_{jk}\Psi_{jk} = \sum_{\ell\ell_1\ell_2}[\varpi_\ell^{(j)}]^2\ I_{\ell_1\ell_2\ell}B_{\ell_1\ell_2\ell}\ b_{\ell_1}b_{\ell_2}b_\ell\ ; \tag{72}$$

$$\beta_j^{(\Psi^2,\nabla^2\Psi)} = \frac{1}{N_{\rm pix}^{(j)}}\sum_k [\Psi^2]_{jk}[\nabla^2\Psi]_{jk} = \sum_{\ell\ell_1\ell_2}[\varpi_\ell^{(j)}]^2\ (\Pi_{\ell_1}+\Pi_{\ell_2}+\Pi_\ell)I_{\ell_1\ell_2\ell}B_{\ell_1\ell_2\ell}\ b_{\ell_1}b_{\ell_2}b_\ell\ ; \tag{73}$$

$$\beta_j^{(\nabla^2\Psi,\nabla\Psi\cdot\nabla\Psi)} = \frac{1}{N_{\rm pix}^{(j)}}\sum_k [\nabla\Psi\cdot\nabla\Psi]_{jk}[\nabla^2\Psi]_{jk} = \sum_{\ell\ell_1\ell_2}[\varpi_\ell^{(j)}]^2\ (\Pi_\ell+\Pi_{\ell_1}-\Pi_{\ell_2})\Pi_{\ell_2}+{\rm cyc.perm.})I_{\ell_1\ell_2\ell}B_{\ell_1\ell_2\ell}\ b_{\ell_1}b_{\ell_2}b_\ell\ . \tag{74}$$

Thus, the three generalized skew-spectra can be obtained simply by cross-correlating the relevant maps in the needlet basis. No specific assumption about the underlying bispectrum is used. Though the primary aim is to study the primordial bispectrum, the results will be equally applicable to that due to the secondaries. The main advantage of using the skew-spectra is related to its ability to probe the NG as a function of angular scale thus retaining the power to discriminate between various models of primaries or secondaries.

Using equation (46), the coefficients of modal decomposition recovered from maps can also be used to estimate directly the skew-spectra in the needlet domain, and results from two different methods can be useful for consistency checks.

In our derivation, we have used the following expression for the needlet bispectrum:

$$\langle\Psi_{j_1k_1}\Psi_{j_2k_2}\Psi_{j_3k_3}\rangle = \sqrt{\lambda_{j_1k_1}}\sqrt{\lambda_{j_2k_2}}\sqrt{\lambda_{j_3k_3}}\sum_{\ell_1\ell_2\ell_3}\varpi_{\ell_1}^{(j_1)}\varpi_{\ell_2}^{(j_2)}\varpi_{\ell_3}^{(j_3)}$$
$$\times\sum_{m_1m_2m_3}Y_{\ell_1m_1}(\hat\Omega_{j_1k_1})Y_{\ell_2m_2}(\hat\Omega_{j_2k_2})Y_{\ell_3m_3}(\hat\Omega_{j_3k_3})\begin{pmatrix}\ell_1 & \ell_2 & \ell_3\\ m_1 & m_2 & m_3\end{pmatrix}B_{\ell_1\ell_2\ell_3}b_{\ell_1}b_{\ell_2}b_{\ell_3}. \tag{75}$$

Finally, we can express the needlet skew-spectra as a convolution of the skew-spectra defined in the harmonic domain.

$$\beta_j^{(\Psi^2,\Psi)} = \sum_\ell \Xi_\ell\ [\varpi_\ell^{(j)}]^2\ S_\ell^{(0)};\qquad \sum_j\beta_j^{(\Psi^2,\Psi)} = \sum_\ell\ \Xi_\ell\ S_\ell^{(0)} = S^{(0)}. \tag{76}$$

Similar results can be obtained relating $\beta_j^{(\Psi^2,\nabla^2\Psi)}$ to $S_\ell^{(1)}$ as well as $\beta_j^{(\nabla\Psi\cdot\nabla\Psi,\nabla^2\Psi)}$ to $S_\ell^{(2)}$. Thus, the needlet skew-spectra are simply *binned harmonic skew-spectra*. The higher order generalization to two-to-two and three-to-one power-spectra can be achieved using the same principle:

$$\beta_j^{(\Psi^2,\Psi^2)} = \frac{1}{N_{\rm pix}^{(j)}}\sum_k[\Psi^2]_{jk}[\Psi^2]_{jk} = \sum_\ell\Xi_\ell[\varpi_\ell^{(j)}]^2K_\ell^{(2,2)} = \sum_\ell[\varpi_\ell^{(j)}]^2\ \sum_{\ell_i}\frac{1}{\Xi_L}I_{\ell_1\ell_2\ell}I_{\ell_3\ell_3\ell}T^{\ell_1\ell_2}_{\ell_3\ell_4}(\ell)b_{\ell_1}b_{\ell_2}b_{\ell_3}b_{\ell_4}; \tag{77}$$

$$\beta_j^{(\Psi^3,\Psi)} = \frac{1}{N_{\rm pix}^{(j)}}\sum_k[\Psi^3]_{jk}[\Psi]_{jk} = \sum_\ell\Xi_\ell[\varpi_\ell^{(j)}]^2K_\ell^{(3,1)}\ = \sum_\ell\ \Xi_\ell\ [\varpi_\ell^{(j)}]^2\sum_{\ell_i\ell}\frac{1}{\Xi_\ell}I_{\ell_1\ell_2\ell}I_{L\ell_3\ell}\ T^{\ell_1\ell_2}_{\ell_3\ell}(\ell)b_{\ell_1}b_{\ell_2}b_{\ell_3}b_\ell. \tag{78}$$

In both cases if we sum over all possible modes, we can recover the kurtosis K_4:

$$\sum_j\beta_j^{\Psi^2,\Psi^2} = \sum_j\beta_j^{\Psi^3,\Psi} = K_4 = \sum_{\ell_i}\sum_\ell I_{\ell_1\ell_2L}I_{\ell_3\ell L}T^{\ell_1\ell_2}_{\ell_3\ell_4}(\ell)b_{\ell_1}b_{\ell_2}b_{\ell_3}b_{\ell_4}. \tag{79}$$

Thus, we arrive at the same one-point kurtosis using a different modal expansion. The generalized kurt-spectra required to construct the MFs have a similar expression:

$$\beta_j^{(i)} = \sum_\ell\Xi_\ell\ [\varpi_\ell^{(j)}]^2\ K_\ell^{(i)};\qquad \sum_j\beta_j^{(i)} = K^{(i)}. \tag{80}$$

The expression that relates $K_\ell^{(i)}$ with the corresponding generalized trispectrum is given in equation (B13). The expressions for the generalized trispectra are given in equations (B10)–(B12).

To perform an error analysis, we note that the error in an arbitrary needlet skew- or kurt-spectrum $\beta_j^{A,B}$ can be expressed as a weighted sum of scatter in respective skew- or kurt-spectra $S_\ell^{(A,B)}$ or $K_\ell^{(A,B)}$:

$$\delta\beta_j^{(A,B)} = \sum_\ell\Xi_\ell[\varpi_\ell^{(j)}]^2\delta S_\ell^{(A,B)}. \tag{81}$$

Using expressions of error-covariance for $\delta S_\ell^{(A,B)}$ or $\delta T_\ell^{(A,B)}$ derived earlier, we can work out similar expressions for the needlet spectra $\delta\beta_j^{(A,B)}$

$$\mathbb{C}_{ij}^{(A,B)} = \sum_\ell\sum_{\ell'}\Xi_\ell[\varpi_\ell^{(i)}]^2\mathfrak{C}_{\ell\ell'}^{(A,B)}\Xi_{\ell'}[\varpi_{\ell'}^{(j)}]^2, \tag{82}$$

with $\mathbb{C}_{ij}^{(A,B)} = \langle\delta\beta_i^{(A,B)}\beta_j^{(A,B)}\rangle$ and $\mathfrak{C}_{\ell\ell'}^{(A,B)} = \langle\delta\mathcal{C}_l^{(A,B)}\delta\mathcal{C}_{l'}^{(A,B)}\rangle$ being the covariance in needlet and harmonic bases.

Table 1. Specification of the filter functions $\varpi_\ell^{(j)}$ used. The functional form is given in equation (83).

j	0	1	2	3	4	5	6	7	8
$\ell_{\rm min}$	0	0	50	100	150	250	350	550	650
$\ell_{\rm max}$	50	100	150	250	350	550	650	800	1000
$\ell_{\rm peak}$	0	50	100	150	250	350	550	650	800

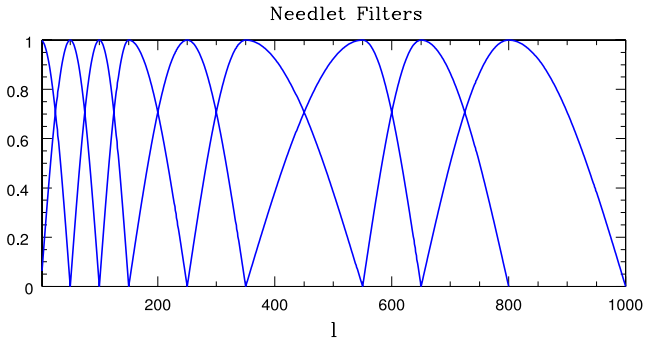

Figure 12. The needlet filters $\varpi_\ell^{(j)}$ defined in equation (61) that correspond to nine different *frequencies j* used in our study are depicted.

A few comments are in order at this point. The cumulant correlators and the series of multispectra such as skew- or kurt spectra represent two-point objects in real space and in the harmonic domain. The statistics developed here are their needlet representation. Throughout the results here ignore odd-*parity* modes. To include the *odd-parity* modes in equations (72)–(74), we can replace $I_{\ell_1\ell_2\ell_3}$ with $\mathcal{I}_{\ell_1\ell_2\ell_3}$ and use $B_{\ell_1\ell_2\ell_3} = b_{\ell_1\ell_2\ell_3}\mathcal{I}_{\ell_1\ell_2\ell_3}$. The discussion in this section does not depend on a specific form of the bispectrum and can be relevant in many other areas in cosmology, e.g. weak lensing or studies regarding galaxy distribution where studies of NG is performed.

The concept of needlets has been extended by Geller & Mayeli (2009a,b) to Mexican needlets by replacing the compactly supported kernel $\varpi_\ell^{(j)}$ with a smooth functional form. Mexican needlets have extremely good localization properties in real space and can be used to approximate the spherical Mexican wavelet at high angular frequencies. Results derived above can be applicable in such situations. It was noticed previously that the needlet-based estimators are generally less affected by anisotropic noise and observational mask (Curto et al. 2011). Further tightening of error-bars of a KSW-based optimized estimator and a linear correction term was reported by Donzelli et al. (2012) which can be adopted in our analysis. The generalization to the case of spinorial fields by using a spin-needlet decomposition (Geller & Marinucci 2010) will be presented elsewhere.

For specific computation of skew-spectra in needlet basis we choose the following functional form Basak & Delabrouille (2012):

$$\varpi_\ell^j = \sin\left[\frac{\ell_{\rm peak}-\ell}{\ell_{\rm peak}-\ell_{\rm min}}\frac{\pi}{2}\right]; \qquad \ell < \ell_{\rm peak};$$
$$\varpi_\ell^j = 1; \qquad \ell = \ell_{\rm peak};$$
$$\varpi_\ell^j = \sin\left[\frac{\ell-\ell_{\rm peak}}{\ell_{\rm max}-\ell_{\rm peak}}\frac{\pi}{2}\right]; \qquad \ell > \ell_{\rm peak}. \tag{83}$$

The choice of $\ell_{\rm min}$, $\ell_{\rm max}$ and $\ell_{\rm peak}$ are tabulated in Table 1 for nine different *frequencies* which are plotted in Fig. 12. The resulting expressions for the skew-spectra in the needlet basis $\beta_j^{\psi^2,\Psi}$, $\beta_j^{\Psi^2,\nabla^2\Psi}$ and $\beta_j^{\nabla\Psi\cdot\nabla\Psi,\nabla^2\Psi}$ are shown in Fig. 13 for *local* and *equilateral* models of primordial NG.

8 DISCUSSION OF RESULTS

Different approaches are essential while testing NG as they all exploit different statistical characteristics. There is no unique approach that can be adopted to describe or parametrize NG in a complete manner. Testing of NG therefore must be done using a battery of complementary techniques, and each of these techniques has a unique response to the real-world issues such as the sky-coverage and instrumental noise. Any robust detection therefore will have to involve a simultaneous cross-validation of results obtain from independent methods.

8.1 Generalized skew-spectra to differentiate different primordial or secondary contribution

One of the main difficulties faced by one-point estimators, which also includes the MF-based approaches, is their inability to differentiate various sources of NG. The one-point estimators typically compress all available information to a single number. If different sources of

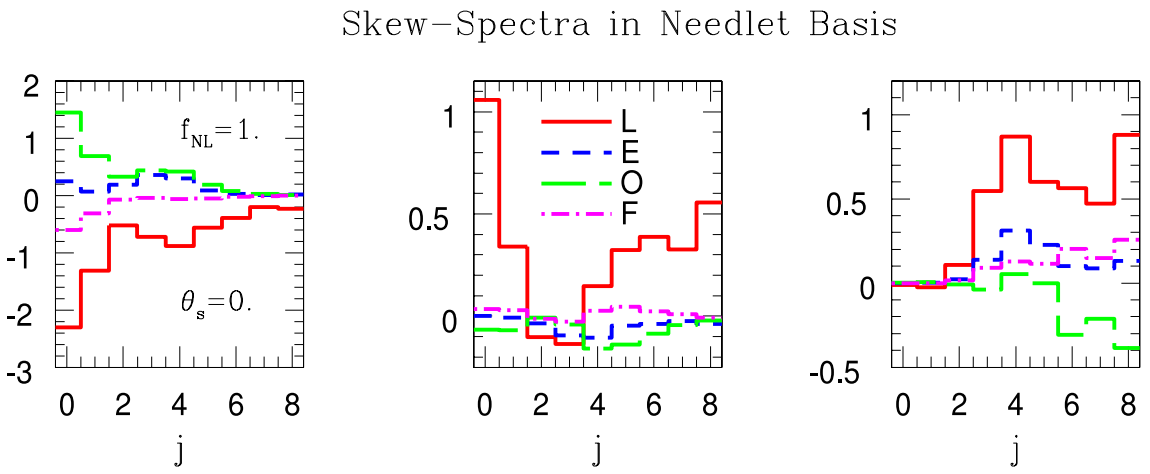

Figure 13. The three different skew-spectra defined in the needlet domain, by equation (76) are shown for the bins defined in Fig. 12. From left to right the different panels correspond to $S_j^{(0)}$, $S_j^{(1)}$ and $S_j^{(2)}$. The lines correspond to the local (L), equilateral (E), orthogonal (O) and folded (F) models of primordial NG. The experimental setup is that of the *Planck* 143 GHz channel and normalization $f_{\rm NL}$ for each model is taken to be unity.

non-Gaussianities are considered simultaneously, then the compression is typically to a set of numbers equal to the number of parameters to be estimated (see e.g. Komatsu et al. 2009), but in this case verification that the non-Gaussian sources probed are actually responsible for the non-Gaussian signals is not possible. This has the advantage of increasing the S/N but it loses the ability to differentiate various sources of NG. In any study of primordial NG, it is of the utmost importance to avoid any cross-contamination from secondary sources (see e.g. Goldberg & Spergel 1999a,b; Cooray & Hu 2000). In recent studies involving MFs, a certain level of disagreement has been noticed with studies that use the bispectrum to probe NG (see e.g. Hikage et al. 2006). Given that MF-based approaches only directly probe the bispectra, as the contributions from the higher order multispectra are subdominant, it is important to understand the reasons for these disagreements.

Following Munshi & Heavens (2010), we have developed a new technique to study the morphology of the CMB sky. Instead of one-point estimators, e.g. the skewness, their method relies on a spectrum or skew-spectrum which is the Fourier transform of two-point objects in real space known as cumulant correlators. These skew-spectra do not compress all available information from the study of a bispectrum to a single number and their shape can help to distinguish among various sources of NG. Exploiting the perturbative expansion of the MFs it can be seen that at the leading order of NG, the MFs depend on three generalized skewness parameters equation (4). We extend the concept of the skew-spectra to the study of these MFs and introduce one generalized skew-spectrum with each of these skewness parameters. This allows us to introduce a power spectrum associated with MFs. The advantage of cross-checking the contributions to MFs using the skew-spectra is that they provide a method to test any contamination from secondaries or foregrounds. The methods based on the skew-spectra are simpler to implement once the derivative maps are constructed. These methods are similar to moment-based approaches for studying NG and hence can provide a valuable basis for cross-comparison. We have shown that this can be implemented in a model-independent way. Our method is based on a pseudo-$\mathcal{C}_\ell$ approach and can handle arbitrary sky coverage and inhomogeneous noise distribution. The pseudo-$\mathcal{C}_\ell$ approach is well understood in the context of power spectrum studies and its variance or scatter can be computed analytically. We provide generic analytical results for computation of scatter around the individual estimates in equations (29)–(31). The level of cross-correlation among various estimators can be estimated using equations (33)–(35).

It is also possible to go beyond the lowest level in NG. However, it is expected that such correction will be subdominant at least in the context of CMB data analysis. Nevertheless, we include the spectrum associated with the next-order correction terms that were introduced by Matsubara (2010). These terms represent kurtosis and the corresponding spectra are known as kurt-spectra. In their study, Munshi et al. (2011a) introduced two sets of kurt-spectra. Adopting their method, we show that generic two-to-two kurt-spectra can be extracted from the data without introducing any additional complication using equations (B14)–(B15). Using a simple model for the bispectrum from unsubtracted points sources (equation 20), it is possible to provide an estimate of cross-contamination from this foreground in estimation of other types of NG.

The one-point generalized skewness parameters $S^{(i)}$ are plotted in Fig. 1. In Fig. 3, we have shown the result of our computation for generalized skew-spectra $S_\ell^{(0)}$, $S_\ell^{(1)}$, $S_\ell^{(2)}$ for various beam sizes θ_s. In Fig. 4, the results for equilateral model are shown, with the corresponding normalization set to unity $f_{\rm NL}^{\rm equi} = 1$ and Fig. 5 and Fig. 6 correspond to orthogonal and enfolded models, respectively. The corresponding results for point sources are depicted in Fig. 7. In Fig. B1, we show the three cumulant correlators corresponding to the *Planck* experiment. The cumulant correlators are real-space representations of the corresponding skew-spectra. We have plotted the S/N for various primordial models of NG in Fig. 8–11 for various non-Gaussian models.

8.2 Generalized skew-spectra in the needlet basis

In addition to their usual harmonic-domain representation and characterization in real space using the cumulant correlators, we have analysed the skew-spectra in the needlet domain. The skew-spectra defined in needlet domain are intermediate between the cumulant correlators

defined in real space and the skew-spectra defined in harmonic domain. It allows localized filtering in real as well as in harmonic domain. In Section 7, we show that the skew-spectra in the needlet domain can be obtained through appropriate filtering of the skew-spectra in the harmonic domain equations (72)–(74). These expressions can be used to construct the MFs in the needlet domain using the expressions for the skewness parameters equation (76). Though mathematically equivalent, use of different bases can be useful for understanding the impact of various systematics.

We also relate both of the kurt-spectra, two-to-two and three-to-one defined in the needlet basis in terms of their counterparts in the harmonic domain in equations (77) and (78), which can both be used to construct the kurtosis using equation (79). The generalized kurt-spectra can also be constructed using similar techniques and are filtered versions of their harmonic counterparts.

Errors in the needlet basis can be related to their harmonic counterparts via equation (31). Estimation of MFs can be done using the HEALPIX-based pipeline that uses publicly available software such as NEEDATOOL (Pietrobon et al. 2010). For the estimation of needlet skew- and kurt-spectrum, we provide a pseudo-$\mathcal{C}_\ell$ based approach.

The needlet filters $\varpi_\ell^{(j)}$ used in our study are presented in Fig. 12. and the needlet skew-spectra $S_j^{(0)}$, $S_j^{(1)}$ and $S_j^{(2)}$ for *Planck*- and EPIC-type experiments are given in fig. C1 and fig. C2, respectively.

8.3 Generalized skew-spectra and modal decomposition

We have used the coefficients from the modal decomposition of bi- or trispectrum equations (40) and (48) to reconstruct the generalized skew- and kurt-spectra. This procedure gives a direct route to reconstruct the morphology of the CMB maps using modal decomposition. The coefficients of modal decomposition are estimated using an orthogonal or separable basis function. This method provides an alternative to the computation of MFs using generalized skew- and kurt-spectra of derivative maps that we have developed in the text of the paper. This method of modal decomposition can work for generic multispectra and thus can be useful to construct MFs or the related skew- or kurt-spectra in diverse cosmological situations.

8.4 Skew-spectra for odd-parity bispectrum

We have also extended the concept of generalized skew-spectra to include the odd-parity bispectrum in equations (51)–(53). This will be useful in probing footprints of parity violating physics in CMB maps. Even in the absence of any known parity-violating physics odd-parity skew-spectra can be useful for detecting systematic effects.

Finally, we note that none of the derivations are based on any specific assumption about the nature of bispectrum. Thus, the generic results derived here will also be applicable to other areas of cosmology where morphological estimators are used to estimate primordial or secondary NG.

9 CONCLUSION

We have generalized the concept of skew-spectra in different basis functions and used it to estimate the MFs. The aim is to define compressed NG statistics which retain information on the nature of the NG. This will allow cross-validation of results obtained using different estimators at various intermediate steps, thus allowing a better handle on any contamination from possible sources of systematics. The results we have derived are independent of any specific assumptions regarding the nature of NG and can be useful in other areas of cosmology. We have also included a contribution from odd-parity bispectrum in our reconstruction of MFs using the skew-spectra.

In addition to these statistics, we have developed an analytical framework which can be useful in estimating the S/N for a given experimental setup (beam and noise). Using this framework, we found that, among the three skew-spectra probed, the S/N is highest for $S_\ell^{(1)}$, with the ordering of $S_\ell^{(0)}$ and $S_\ell^{(2)}$ being model dependent. We have tested four different models of NG. We find the estimators $S_\ell^{(0)}$ and $S_\ell^{(1)}$ are highly anticorrelated beyond $\ell = 30$ with a coefficient of correlation $r_\ell^{01} \approx -1$ for primordial NG. We found moderate correlation between $S_\ell^{(0)}$ and $S_\ell^{(2)}$ as well as $S_\ell^{(1)}$ and $S_\ell^{(2)}$ with $r_{02} \approx -0.5$ and $r_{12} \approx 0.5$ at $\ell \approx 1500$. We found the cumulative S/N on $f_{\rm NL}$ to be $\approx$0.1 for the local model for $f_{\rm NL} = 1$, scaling roughly proportionally to $f_{\rm NL}$. The S/N can be improved by using *Wiener-filtered* maps as inputs, and the results presented here can be generalized to take into account such improvements.

The MFs provide a complementary tool to moment-based approaches in real space or equivalently multispectral analysis in the harmonic domain. Our results also provide an unifying approach in different bases including in needlet basis. Note that our S/N results depend on various simplifying approximations that allow analytical treatment; e.g. we have not included position-dependent noise, which will involve hit-count maps, but recent studies have found the MFs to be rather insensitive to such detailed modelling (Ducout et al. 2012). We have adopted an $f_{\rm sky}$ approach for dealing with partial sky coverage; detailed modelling will involve exact calculation of mode–mode coupling, i.e. characterization of galactic as well as a point source mask. In our derivation of scatter, we have ignored all higher order correlations, which can always be characterized using numerical Monte Carlo simulations. We do not include biases from secondaries which can generate spurious signatures independently or through its coupling to primaries, e.g. generated by the ISW effect at large angular scales or from the lensing and tSZ cross-correlation at smaller angular scales; both can provide detectable observable signatures.

The skew-spectra that we have studied are mildly suboptimal. However, we have developed generic reconstruction procedure for the MFs using optimal modal decomposition techniques that is typically used for construction of an optimum estimator. We also extend the method beyond the bispectrum to take into account higher order corrections to the level of trispectrum e.g. from lensing of primary CMB.

ACKNOWLEDGEMENTS

DM acknowledges support from STFC standard grant ST/G002231/1 at School of Physics and Astronomy at Cardiff University where this work was completed. AC and JS are supported by NSF-AST0645427 and NASA NNX10AD42G. DM would like to thank Michele Liguori for useful discussions. We would like to thank an anonymous referee for many useful suggestions.

REFERENCES

Acquaviva V., Bartolo N., Matarrese S., Riotto A., 2003, Nucl. Phys. B, 667, 119
Antoine J.-P., Vandergheynst P., 1999, Appl. Comput. Harmon. Anal., 7, 262
Babich D., 2005, Phys. Rev. D, 72, 043003
Bartolo N., Komatsu E., Matarrese S., Riotto A., 2004, Phys. Rep. 402, 103
Bartolo N., Matarrese S., Riotto A., 2006, J. Cosmol. Astropart. Phys., 06, 024
Basak S., Delabrouille J., 2012, MNRAS, 419, 1163
Byrnes C. T., Choi K.-Y., 2010, Adv. Astron., 2010, 724525
Byrnes C. T., Sasaki M., Wands D., 2006, Phys. Rev. D, 74, 123519
Cabella P., Hansen F., Marinucci D., Pagano D., Vittorio N., 2004, Phys. Rev. D, 69 063007
Cabella P., Hansen F. K., Liguori M., Marinucci D., Matarrese S., Moscardini L., Vittorio N., 2006, MNRAS, 369, 819
Cabella P., Natoli P., Silk J., 2007, Phys. Rev. D, 76, 123014
Caroll S. M., 1998, Phys. Rev. Lett., 81, 3067
Caroll S. M., Field G. B., Jackiw R., 1990, Phys. Rev. D, 41, 1231
Chen X., Huang M., Kachru S., Shiu G., 2007a, J. Cosmol. Astropart. Phys., 01, 002
Chen X., Easther R., Lim E. A., 2007b, J. Cosmol. Astropart. Phys., 06, 023
Cooray A., 2001, Phys. Rev. D, 64, 043516
Cooray A. R., Hu W., 2000, ApJ, 534, 533
Creminelli P., 2003, J. Cosmol. Astropart. Phys., 10, 003
Creminelli P., Nicolis A., Senatore L., Tegmark M., Zaldarriaga M., 2006, J. Cosmol. Astropart. Phys., 5, 4
Creminelli P., Senatore L., Zaldarriaga M., Tegmark M., 2007a, J. Cosmol. Astropart. Phys., 3, 5
Creminelli P., Senatore L., Zaldarriaga M., 2007b, J. Cosmol. Astropart. Phys., 3, 19
Curto A., Martinez-Gonzalez E., Barreiro B., Hobson M. P., 2011, MNRAS, 412, 1038
Donzelli S., Hansen F. K., Liguori M., Marinucci D., Matarrese S., 2012, ApJ, 755, 19
Ducout A., Bouchet F., Colombi S., Pogosyan D., Prunet S., 2012, MNRAS, 429, 2104
Edmonds A. R., 1968, Angular Momentum in Quantum Mechanics, 2nd edn. Princeton Univ. Press, Princeton
Eriksen H. K., Novikov D. I., Lilje P. B., Banday A. J., Gorski K. M., 2004, ApJ, 612, 64
Falk T., Madden R., Olive K. A., Srednicki M., 1993, Phys. Lett. B, 318, 354
Feng B., Li M., Xia J.-Q., Chen X., Zhang X., 2006, Phys. Rev. Lett., 96, 221302
Fergusson J. R., Liguori M., Shellard E. P. S, 2010a, Phys. Rev. D, 82, 3502
Fergusson J. R., Regan D. M., Shellard E. P. S., 2010b, preprint (arXiv:1012.6039)
Freeden W., Schneider F., 1998, Inverse Probl., 14, 225
Gangui A., Lucchin F., Matarrese S., Mollerach S., 1994, ApJ, 430, 447
Geller D., Marinucci D., 2010, preprint (arXiv:1006.3835)
Geller D., Mayeli A., 2009a, Math. Z., 262, 895
Geller D., Mayeli A., 2009b, Math. Z., 263, 235
Goldberg D. M., Spergel D. N., 1999a, Phys. Rev. D, 59, 103001
Goldberg D. M., Spergel D. N., 1999b, Phys. Rev. D, 59, 103002
Guilloux F., Fay G., Cardoso J.-F., 2007, preprint (arXiv:0706.2598v1)
Gupta S., Berera A., Heavens A. F., Matarrese S., 2002, Phys. Rev. D, 66, 043510
Hadwiger H., 1959, Math. Z., 71, 124
Hansen F. K., Banday A. J., Eriksen H. K., Gorski K. M., Lilje P. B., 2006, ApJ, 648, 784
Heavens A. F., 1998, MNRAS, 299, 805
Hikage C., Matsubara T., 2012, MNRAS, 425, 2187
Hikage C. et al., 2002, PASJ, 54, 707
Hikage C., Taruya A., Suto Y., 2003, PASJ, 55, 335
Hikage C., Komatsu E., Matsubara T., 2006, ApJ., 653, 11
Hikage C., Coles P., Grossi M., Moscardini L., Dolag K., Branchini L., Matarrese S., 2008a, MNRAS, 385, 1513
Hikage C., Matsubara T., Coles P., Liguori M., Hansen F. K., Matarrese S., 2008b, MNRAS, 389, 1439
Hivon E., Górski K. M., Netterfield C. B., Crill B. P., Prunet S., Hansen F., 2002, ApJ, 567, 2
Hu W., 2000, Phys. Rev. D, 62, 043007
Hu W., 2001, Phys. Rev. D, 64, 083005
Hu W., Okamoto T., 2002, ApJ, 574, 566
Kamionkowski M., Souradeep T., 2011, Phys. Rev. D, 83, 027301
Kamionkowski K., Smith T., Heavens A., 2011, Phys. Rev. D, 83, 023007
Kermish Z. et al., 2012, Proc. SPIE, 8452, 84521C
Kogo N., Komatsu E., 2006, Phys. Rev. D, 73, 083007
Komatsu E., 2010, Classical Quantum Gravity, 27, 124010
Komatsu E., Spergel D. N., 2001, Phys. Rev. D, 63, 3002
Komatsu E. et al., 2001, ApJS, 192, 18

Komatsu E., Wandelt B. D., Spergel D. N., Banday A. J., Górski K. M., 2002, ApJ, 566, 19
Komatsu E. et al., 2003, ApJS, 148, 119
Komatsu E., Spergel D. N., Wandelt B. D., 2005, ApJ, 634, 14 (KSW)
Komatsu E. et al., 2009, ApJS, 180, 330
Larson D. et al., 2010, ApJS, 192, 16
Liguori M., Yadav A., Hansen F. K., Komatsu E., Matarrese S., Wandelt B., 2007, Phys. Rev. D, 76, 105016
Linde A. D., Mukhanov V. F., 1997, Phys. Rev. D, 56, 535
Lue A., Wang L. M., Kamionkowski M., 1990, Phys. Rev. Lett., 83, 1506
Lyth D. H., Ungarelli C., Wands D., 2003, Phys. Rev. D, 67, 023503
Maldacena J. M., 2003, J. High Energy Phys., 05, 013
Marinucci D. et al., 2008, MNRAS, 383, 539
Matsubara T., 2003, ApJ, 584, 1
Matsubara T., Jain B., 2001, ApJ, 552, L89
Matsubara T., 2010, Phys. Rev. D, 81, 083505
McEwen J. D., Hobson M. P., Lasenby A. N., 2006, preprint (astro-ph/0609159)
McEwen J. D., Vielva P., Hobson M. P., Martinez-Gonzalez E., Lasenby A. N., 2007, MNRAS, 376, 1211
McMahon J. et al., 2009, in Young B., Cabrera B., Miller A., eds, AIP Conf. Ser. Vol. 1185, SPTpol: An Instrument for CMB Polarization. Am. Inst. Phys., New York, p. 511
Mecke K. R., Buchert T., Wagner H., 1994, A&A, 288, 697
Medeiros J., Contaldi C. R., 2006, MNRAS, 367, 39
Meerburg P. D., van der Schaar J. P., Corasaniti P. S., 2009, J. Cosmol. Astropart. Phys., 05, 018
Moss I., Xiong C., 2007, J. Cosmol. Astropart. Phys., 04, 007
Moudden Y., Cordoso J. F., Starck J. L., Delabrouille J. , 2003, J. Appl. Signal Process, 15, 2473
Munshi D., Heavens A., 2010, MNRAS, 401, 2406
Munshi D., Souradeep T., Starobinsky A. A., 1995, ApJ, 454, 552
Munshi D., Heavens A., Cooray A., Smidt J., Coles P., Serra P., 2011a, MNRAS, 412, 1993
Munshi D., Valageas P., Cooray A., Heavens A., 2011b, MNRAS, 414, 3173
Munshi D., Smidt J., Joudaki S., Coles P., 2012a, MNRAS, 419, 138
Munshi D., van Waerbeke L., Smidt J., Coles P., 2012b, MNRAS, 419, 536
Munshi D., Coles P., Heavens A., 2013, MNRAS, 428, 2628
Narcowich F. G., Peterushev P., Ward J. D., 2006, SIAM J. Math Anal., 38., 574
Natoli P. et al., 2010, MNRAS, 408, 1658
Niemack M. D. et al., 2010, Proc. SPIE, 7741, 77411S
Novikov D., Schmalzing J., Mukhanov V. F., 2000, A&A, 364, 17
Park C. et al., 2005, ApJ, 633, 11
Pietrobon D., Balbi A., Marinucci D., 2006, Phys. Rev. D, 74, 043524
Pietrobon D., Amblard A., Balbi A., Cabella P., Cooray A., Marinucci D., 2008, Phys. Rev. D, 78, 103504
Pietrobon D., Balbi A., Cabella P., Gorski K. M., 2010, ApJ, 723, 1
Planck Collaboration, 2013, preprint (arXiv:1303.5084)
Pratten G., Munshi D., 2012, MNRAS, 423, 3209
Regan D. M., Shellard E. P. S., 2010, Phys. Rev. D, 82, 3527
Regan D. M., Shellard E. P. S., Fergusson J. R., 2010, Phys. Rev. D, 82, 3520
Rudjord O., Hansen F. K., Lan X., Liguori M., Marinucci D., Matarrese S., 2009, ApJ, 701, 369
Salopek D. S., Bond J. R., 1990, Phys. Rev. D, 42, 3936
Salopek D. S., Bond J. R., 1991, Phys. Rev. D, 43, 1005
Santos M. G. et al., 2003, MNRAS, 341, 623
Sanz J. L., Herranz D., Lopez-Caniego M., Argueso F., 2006, in Gini F., Kuruoglu E. E., eds, Proc. 14th EUSIPCO 2006, Wavelets on the Sphere. Application to the Detection Problem. University of Pisa, Italy, p. 5
Sasaki M., V Valiviita J., Wands D., 2006, Phys. Rev. D, 74, 103003
Schmalzing J., Buchert T., 1997, ApJ, 482, L1
Schmalzing J., Gośrski K. M., 1998, MNRAS, 297, 355
Schmalzing J., Takada M., Futamase T., 2000, ApJ, 544, L83
Smidt J., Amblard A., Byrnes C. T., Cooray A., Heavens A., Munshi D., 2010, Phys. Rev. D, 81, 123007
Smith K. M., Zaldarriaga M., 2011, MNRAS, 417, 2
Smith K. M., Zahn O., Dore O., 2007, Phys. Rev. D, 76, 043510
Smith K. M., Senatore L., Zaldarriaga M., 2009, J. Cosmol. Astropart. Phys., 09, 006
Spergel D. N. et al., 2007, ApJS, 170, 377
Starck J.-L., Mouden Y., Abrial P., Nguyen M., 2006, A&A, 446, 1191
Taruya A., Takada M., Hamana T., Kayo I., Futamase T., 2002, ApJ, 571, 638
Tauber J. A. et al., 2010, A&A, 520, 1
The COrE Collaboration, 2011, preprint (arXiv:1102.2181)
Tomita H., 1986, Prog. Theor. Phys., 76, 952
Verde L., Wang L., Heavens A., Kamionkowski M., 2000, MNRAS, 313, L141
Vielva P., Martinez-Gonzalez E, Barreiro R. B., Sanz J. L., Cayon L., 2004, ApJ, 609, 22
Wang L., Kamionkowski M., 2001, Phys. Rev. D, 61, 3504
Winitizki S., Kosowsky A., 1998, New Astron., 3, 75
Wu E. Y. S. (QUAD collaboration), 2009, Phys. Rev. Lett., 102, 161302
Yadav A. P. S., Wandelt B. D., 2010, Adv. Astron., 2010, 565248

Yadav A. P. S., Komatsu E., Wandelt B. D., 2007, ApJ, 664, 680
Yadav A. P. S., Komatsu E., Wandelt B. D., Liguori M., Hansen F. K., Matarrese S., 2008, ApJ, 678, 578

APPENDIX A: MFs AND THE CMB SKY

The discussion in the main text has been completely generic and is applicable to an arbitrary random 2D map on the surface of the sky. We will specialize the discussion in this section to the case of CMB the cleanest probes of primordial NG (Planck Collaboration 2013), although the level of NG is highly constrained by observation.

The angular multispectra for the temperature fluctuations sample the 3D multispectra of the inflationary potential. Given a specific form for the primordial NG, it is possible to compute the MFs for the observed temperature perturbations. The NG in the CMB sky can be a direct manifestation of the NG in the seed perturbations generated during inflation. The NG in the inflationary potential is most easily characterized in the Fourier domain, $\Phi(\boldsymbol{k})$. The following expression links the curvature fluctuations $\Phi(\boldsymbol{k})$ with spherical harmonic coefficients of the temperature anisotropy $a_{\ell m}$, with the help of the radiation transfer function $\Delta_l(k)$ for the temperature fluctuations (Wang & Kamionkowski 2000). The angular power spectrum for the temperature fluctuations $\mathcal{C}_\ell = \langle a_{\ell m} a^*_{\ell m}\rangle$ can be expressed in terms of the power spectrum of the 3D perturbations in the potential field $\langle \Phi(\boldsymbol{k}_1)\Phi(\boldsymbol{k}_2)\rangle = (2\pi)^3\delta_{3\rm D}(\boldsymbol{k}_1+\boldsymbol{k}_2)P_\Phi(k_1)$

$$a_{\ell m} = 4\pi(-i)^\ell \int \frac{{\rm d}^3k}{(2\pi)^3}\Phi(k)\Delta_\ell(k)Y_{\ell m}(\hat{k}); \quad \mathcal{C}_\ell = \frac{2}{\pi}\int k^2{\rm d}k\, P_\Phi(k)\Delta^2_\ell(k). \tag{A1}$$

A Gaussian sky can be described statistically just by its angular power spectrum $\mathcal{C}_\ell$. The lowest order departure from the Gaussianity is described by the angular bispectrum. The general form for the 3D bispectrum for the inflationary potential Φ is given as $B_\Phi(k_1, k_1, k_3) = (2\pi)^3\delta_{3\rm D}(\boldsymbol{k}_1+\boldsymbol{k}_2+\boldsymbol{k}_3)\, F_\Phi(k_1, k_2, k_3)$. In general, translational invariance enforces momentum conservation in the Fourier domain leading to the 3D Dirac delta function $\delta_{3\rm D}$. The kernel $F_\Phi(k_1, k_2, k_3)$ therefore is the amplitude of the bispectrum associated with each triangular configurations involving the wavevectors $\boldsymbol{k}_i$. Various early Universe scenarios differ in $F_\Phi(k_1, k_2, k_3)$. The reduced angular bispectrum defined in equation (13) can be expressed in terms of $F_\Phi(k_1, k_2, k_3)$:

$$b_{\ell_1\ell_2\ell_3} = \left(\frac{2}{\pi}\right)^3 \int {\rm d}r r^2 \int k_1^2{\rm d}k_1\, j_{\ell_1}(k_1r)\Delta_{\ell_1}(k_1r)\int k_2^2\,{\rm d}k_2\, j_{\ell_2}(k_2r)\Delta_{\ell_2}(k_2r)\int k_3^2\,{\rm d}k_3\, j_{\ell_3}(k_3r)\Delta_{\ell_3}(k_3r)F_\Phi(k_1, k_2, k_3). \tag{A2}$$

Models of inflation can largely be divided into four different categories. The first class of models is known as the local model (Salopek & Bond 1990; Verde et al. 2000; Komatsu & Spergel 2001; Creminelli 2003; Cabella et al. 2006; Creminelli et al. 2006; Medeiros & Contaldi 2006; Liguori et al. 2007; Smith et al. 2009) and appears in multifield models. In these models, the contribution to the bispectrum is maximum for the squeezed configurations, i.e. when $k_1 \ll k_2, k_3$. The other main class of models are called equilateral models (Chen et al. 2007a,b). In this class of models, the maximum contribution corresponds to a configuration where all wavevectors have similar magnitudes $k_1 \sim k_2 \sim k_3$. It is important to note that unlike the local model the equilateral model cannot be represented by product of separable functions. However, approximate separable forms do exist in the literature (Creminelli et al. 2006; Smith & Zaldarriaga 2006). Note that the local and equilateral forms are nearly orthogonal to each other and hence can be measured nearly independently of each other. The other two models are known as *orthogonal* and *enfolded* models, respectively. The orthogonal model describes NG in single-field models with a non-canonical kinetic term and is nearly orthogonal to both the local and equilateral models. The enfolded model is relevant for models with non-Bunch–Davies vacuum or general higher derivative interactions. We quote the results for the CMB NG here, which arises in the context of local, equilateral, orthogonal and enfolded models. For more details see e.g. Komatsu & Spergel (2001), Komatsu (2010) and Yadav & Wandelt (2010),

$$b^{\rm loc}_{\ell_1\ell_2\ell_3} = 2f_{\rm NL}\int r^2{\rm d}r[\beta_{\ell_1}(r)\beta_{\ell_2}(r)\alpha_{\ell_3}(r) + 2\ \text{cyc.perm.}]; \tag{A3}$$

$$b^{\rm equi}_{\ell_1\ell_2\ell_3} = 6f^{\rm eq}_{\rm NL}\int r^2{\rm d}r[-(\alpha_{\ell_1}(r)\beta_{\ell_2}(r)\beta_{\ell_3}(r) + 2\ \text{cyc.perm.}) - 2\delta_{\ell_1}(r)\delta_{\ell_2}(r)\delta_{\ell_3}(r) + (\beta_{\ell_1}(r)\gamma_{\ell_2}(r)\delta_{\ell_3}(r) + 5\ \text{cyc.perm.})]; \tag{A4}$$

$$b^{\rm ortho}_{\ell_1\ell_2\ell_3} = 6f^{\rm ortho}_{\rm NL}\int r^2{\rm d}r[-3(\alpha_{\ell_1}(r)\beta_{\ell_2}(r)\beta_{\ell_3}(r) + 2\ \text{cyc.perm.}) - 8\delta_{\ell_1}(r)\delta_{\ell_2}(r)\delta_{\ell_3}(r) + (3\beta_{\ell_1}(r)\gamma_{\ell_2}(r)\delta_{\ell_3}(r) + 5\ \text{cyc.perm.})]; \tag{A5}$$

$$b^{\rm en}_{\ell_1\ell_2\ell_3} = 6f^{\rm en}_{\rm NL}\int r^2{\rm d}r[(\alpha_{\ell_1}(r)\beta_{\ell_2}(r)\beta_{\ell_3}(r) + 2\ \text{cyc.perm.}) + 3\delta_{\ell_1}(r)\delta_{\ell_2}(r)\delta_{\ell_3}(r) - (\beta_{\ell_1}(r)\gamma_{\ell_2}(r)\delta_{\ell_3}(r) + 5\ \text{cyc.perm.})]. \tag{A6}$$

The following functions, as used above, are useful in analytical expressions for the bispectrum and trispectrum (Creminelli et al. 2006):

$$\alpha_\ell(r) = \frac{2}{\pi}\int k^2{\rm d}k j_\ell(kr)\Delta_\ell(k); \quad \beta_\ell(r) = \frac{2}{\pi}\int k^2{\rm d}k\, P_\Phi(k) j_\ell(kr)\Delta_\ell(k); \tag{A7}$$

$$\gamma_\ell(r) = \frac{2}{\pi}\int k^2{\rm d}k\, P^{1/3}_\Phi(k) j_\ell(kr)\Delta_\ell(k); \quad \delta_\ell(r) = \frac{2}{\pi}\int k^2{\rm d}k\, P^{2/3}_\Phi(k) j_\ell(kr)\Delta_\ell(k); \tag{A8}$$

$$F_L(r_1, r_2) = \frac{2}{\pi}\int k^2{\rm d}k\, P^{2/3}_\Phi(k) j_\ell(kr_1) j_\ell(kr_2). \tag{A9}$$

Here, j_ℓ is a spherical Bessel function, and $\Delta_\ell(k)$ is the radiation transfer function which can be computed using the publicly available software such as CAMB[10] or CMBFAST.[11] In addition to the bispectra, the *reduced* CMB trispectrum in the local model can be expressed in terms of these functions as

$$\tau^{\ell_1\ell_2}_{\ell_3\ell_4}(\ell) = 4 f^2_{\rm NL} h_{\ell_1\ell_2\ell} h_{\ell_3\ell_4\ell} \int r_1^2 {\rm d}r_1 \int r_2^2 {\rm d}r_2 F_\ell(r_1, r_2) \alpha_{\ell_1}(r_1)\beta_{\ell_2}(r_1)\alpha_{\ell_3}(r_2)\beta_{\ell_4}(r_2)$$
$$+ g_{\rm NL} h_{\ell_1\ell_2 L} h_{\ell_3\ell_4 L} \int r^2 {\rm d}r \beta_{\ell_2}(r)\beta_{\ell_4}(r)[\mu_{\ell_1}(r)\beta_{\ell_3}(r) + \mu_{\ell_3}(r)\beta_{\ell_1}(r)]. \quad \text{(A10)}$$

The above equation is derived from the following expression for the 3D trispectrum for the inflationary potential Φ:

$$\langle \Phi(k_1)\Phi(k_2)\Phi(k_3)\Phi(k_4)\rangle = (2\pi)^3 \delta_{\rm 3D}(\boldsymbol{k}_1 + \boldsymbol{k}_2 + \boldsymbol{k}_3 + \boldsymbol{k}_4) \Big\{ \frac{25}{9} \tau_{\rm NL} \left[P_\Phi(k_1)P_\Phi(k_2)P_\Phi(k_{13}) + 11 \text{ cyc.perm.} \right]$$
$$+ 6\, g_{\rm NL} \left[P_\Phi(k_1)P_\Phi(k_2)P_\Phi(k_3) + 3 \text{ cyc.perm.} \right] \Big\}; \qquad k_{ij} \equiv |\boldsymbol{k}_i + \boldsymbol{k}_j|. \quad \text{(A11)}$$

Assuming a curvature perturbation and standard local form one can derive $\tau_{\rm NL} = (6 f^{\rm loc}_{\rm NL}/5)^2$. However, in a general inflationary scenario $\tau_{\rm NL}$ can be larger. Constraints on $\tau_{\rm NL}$ and $g_{\rm NL}$ were derived (Fergusson, Regan & Shellard 2010b; Smidt et al. 2010) using *WMAP*5 data. Planck collaboration (2013) used maps from the nominal mission to constrain $\tau_{\rm NL}$ and found $\tau_{\rm NL} < 2800$ (95 per cent CL). For detailed discussions about various issues related to the symmetries and modelling of the CMB trispectrum, see Hu & Okamoto (2002), Hu (2000), Hu (2001), Komatsu & Spergel (2001) and Kogo & Komatsu (2006).

APPENDIX B: THE QUADRUPLET OF KURT-SPECTRA AND NEXT-TO-LEADING-ORDER CORRECTIONS

The recent results from *Planck* satellite (Planck Collaboration 2013) indicate a low values of $f_{\rm NL}$ that characterize different models of primordial bispectrum. This motivates us to go beyond the lowest level of NG and use the next-to-leading-order trispectrum and the related quadruplet of kurt-spectra. Indeed, several inflationary scenarios exist in which the bispectrum is suppressed, and the trispectrum is the leading-order NG in the data (Byrnes, Sasaki & Wands 2006; Sasaki, Valiviita & Wands 2006; Byrnes & Choi 2010). A detection of trispectra thus would be a very important validation of such models. It is also important to realize that unlike one-point estimators, the kurt-spectra can separate out the amplitudes $\tau_{\rm NL}$, $g_{\rm NL}$ of two different types of topological diagrams, *snakes* and *stars*, which contribute at the level of the trispectrum (see equation A11). This is interesting given recent that *Planck* results currently only constrain $\tau_{\rm NL}$ and not $g_{\rm NL}$. From a different perspective, the kurt-spectra can also be extremely useful in probing the lensing-induced topology changes that appear at the level of the trispectrum.

In a perturbative analysis, the leading-order terms that signify NG in the analysis of MFs depend on the bispectrum or equivalently a set of skewness terms. The next-to-leading-order correction terms depend on a set of *kurtosis* parameters $K^{(i)}$ that are fourth-order statistics and are analogues of the skewness parameters $S^{(i)}$ which we have defined above. In general, the kurtosis parameters are collapsed fourth-order one-point cumulants and probe the trispectrum with varying weights (see Munshi et al. 2011a for a more detailed discussion on fourth-order one-point cumulants, their two-point counterparts, the cumulant correlators and the related harmonic-space statistics). The four different kurtosis parameters that are related to the MFs are a natural generalization of the ordinary kurtosis $K^{(0)}$ which is routinely applied in many cosmological studies. We will denote these generalized kurtosis parameters by $K^{(i)}$; $i = 1, 2, 3$. These parameters are constructed from the derivative field of the original map $\Psi(\hat{\Omega})$ and its derivatives $\nabla\Psi(\hat{\Omega})$ and $\nabla^2\Psi(\hat{\Omega})$ as follows:

$$K^{(0)} \equiv \frac{1}{\sigma_0^6} K^{(\Psi^4)} = \frac{\langle \Psi^4 \rangle_c}{\sigma_0^6}; \quad K^{(1)} \equiv \frac{1}{\sigma_0^4\sigma_1^2} K^{(\Psi^3\nabla^2\Psi)} = \frac{\langle \Psi^3\nabla^2\Psi \rangle_c}{\sigma_0^4\sigma_1^2}; \quad \text{(B1)}$$

$$K^{(2)} \equiv K^{(2a)} + K^{(2b)} \equiv \frac{2}{\sigma_0^2\sigma_1^4} K^{(\Psi|\nabla\Psi|^2\nabla^2\Psi)} + \frac{1}{\sigma_0^2\sigma_1^4} K^{(|\nabla\Psi|^4)} = 2\frac{\langle \Psi|(\nabla\Psi)|^2(\nabla^2\Psi)\rangle_c}{\sigma_0^2\sigma_1^4} + \frac{\langle |(\nabla\Psi)|^4\rangle_c}{\sigma_0^2\sigma_1^4}; \quad \text{(B2)}$$

$$K^{(3)} \equiv \frac{1}{2\sigma_0^2\sigma_1^4} K^{(|\nabla\Psi|^4)} = \frac{\langle |\nabla\Psi|^4 \rangle_c}{2\sigma_0^2\sigma_1^4}. \quad \text{(B3)}$$

The subscript $_c$ corresponds to the connected components; Gaussian contributions are subtracted out, including both noise and signal. The evaluation of these moments is relatively easy in real space for a pixelized map, and involves taking derivatives of beam-smoothed maps. The corresponding power spectra associated with these fourth-order moments are constructed by cross-correlating appropriate maps in the harmonic domain and are easy to implement numerically [equation (B15) provides exact expressions for the corresponding power spectra or the kurt-spectra].

[10] http://camb.info/
[11] http://www.cmbfast.org/

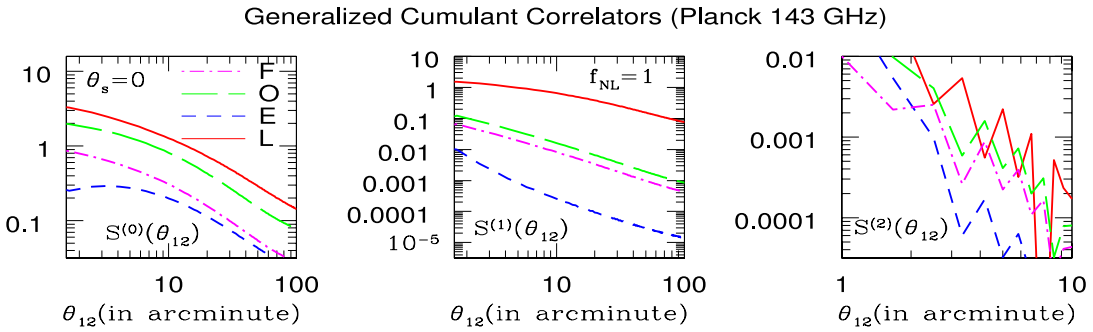

Figure B1. The cumulant correlators defined in equations (15)–(17) are plotted as a function of the separation angle θ_{12} (in arcminute) for the various models of NG for *Planck* (143 GHz channel) experiment as indicated. The cumulant correlators and the corresponding skew-spectra carry equivalent information. Various models of primordial NG considered are *local* (L), *equilateral* (E), *enfolded* (F) and *orthogonal* (O).

The next-to-leading-order corrections to the MFs involve these $K^{(i)}$s as well as the product of two skewness parameters $S^{(i)}$ (i.e. the terms such as $[S^{(0)}]^2$, $[S^{(0)}S^{(1)}]$ or $[S^{(1)}S^{(2)}]$) defined previously in the context of leading-order non-Gaussian terms (Matsubara 2010). The next-to-leading-order corrections $v_k^{(3)}(\nu)$ introduced in equation (3) can be expressed as follows:

$$v_0^{(3)}(\nu) = \frac{[S^{(0)}]^2}{72}\mathcal{H}_5(\nu) + \frac{K^{(0)}}{24}\mathcal{H}_3(\nu); \tag{B4}$$

$$v_1^{(3)}(\nu) = \frac{[S^{(0)}]^2}{72}\mathcal{H}_6(\nu) + \left[\frac{K^{(0)} - S^{(0)}S^{(1)}}{24}\right]\mathcal{H}_4(\nu) - \frac{1}{12}\left[K^{(1)} + \frac{3}{8}[S^{(1)}]^2\right]\mathcal{H}_2(\nu) - \frac{1}{8}K^{(3)} \tag{B5}$$

$$v_2^{(3)}(\nu) = \frac{[S^{(0)}]^2}{72}\mathcal{H}_7(\nu) + \left[\frac{K^{(0)} - 2S^{(0)}S^{(1)}}{24}\right]\mathcal{H}_5(\nu) - \frac{1}{6}\left[K^{(1)} + \frac{1}{2}S^{(0)}S^{(2)}\right]\mathcal{H}_3(\nu) - \frac{1}{2}\left[K^{(2)} + \frac{1}{2}S^{(1)}S^{(2)}\right]\mathcal{H}_1(\nu). \tag{B6}$$

The analytical modelling of four-point correlation functions is most naturally done in the harmonic domain. They are described by the angular trispectrum $T^{\ell_1\ell_2}_{\ell_3\ell_4}(\ell)$, which is defined through the relation

$$\langle a_{\ell_1 m_1} a_{\ell_2 m_2} a_{\ell_3 m_3} a_{\ell_4 m_4}\rangle_c = \sum_{\ell m}(-)^M \begin{pmatrix} \ell_1 & \ell_2 & \ell \\ m_1 & m_2 & m \end{pmatrix}\begin{pmatrix} \ell_3 & \ell_4 & \ell \\ m_3 & m_4 & -m \end{pmatrix} T^{\ell_1\ell_2}_{\ell_3\ell_4}(\ell). \tag{B7}$$

The trispectrum $T^{\ell_1\ell_2}_{\ell_3\ell_4}(\ell)$ is expressed in terms of the pairing function $P^{\ell_1\ell_2}_{\ell_3\ell_4}(\ell)$, encoding all possible inherent symmetries (Hu 2001).

$$T^{\ell_1\ell_2}_{\ell_3\ell_4}(\ell) = P^{\ell_1\ell_2}_{\ell_3\ell_4}(\ell) + \Xi_\ell\left[\sum_{\ell'}(-1)^{\ell_2+\ell_3}\begin{Bmatrix} \ell_1 & \ell_2 & \ell \\ \ell_4 & \ell_3 & \ell' \end{Bmatrix} P^{\ell_1\ell_3}_{\ell_2\ell_4}(\ell') + \sum_{\ell'}(-1)^{\ell+\ell'}\begin{Bmatrix} \ell_1 & \ell_2 & \ell \\ \ell_3 & \ell_4 & \ell' \end{Bmatrix} P^{\ell_1\ell_4}_{\ell_3\ell_2}(\ell')\right]. \tag{B8}$$

The matrices in curly brackets are 6*j* symbols which are defined using 3*j* symbols (see Edmonds 1968 for more detailed discussions). The entities $P^{\ell_1\ell_2}_{\ell_3\ell_4}(\ell)$ can be further decomposed in terms of the *reduced* function $\tau^{\ell_1\ell_2}_{\ell_3\ell_4}(\ell)$:

$$P^{\ell_1\ell_2}_{\ell_3\ell_4}(\ell) = \tau^{\ell_1\ell_2}_{\ell_3\ell_4}(\ell) + (-1)^{\Sigma_U}\tau^{\ell_2\ell_1}_{\ell_3\ell_4}(\ell) + (-1)^{\Sigma_L}\tau^{\ell_1\ell_2}_{\ell_4\ell_3}(\ell) + (-1)^{\Sigma_L+\Sigma_U}\tau^{\ell_2\ell_1}_{\ell_4\ell_3}(\ell); \quad \Sigma_U = \ell_1+\ell_2+\ell; \quad \Sigma_L = \ell_3+\ell_4+\ell. \tag{B9}$$

Each individual model for primordial NG makes a specific prediction for the *reduced* trispectrum which can be used as a fingerprint to rule out many possibilities.

Next, we will introduce three additional trispectra that are constructed using different weights to the original trispectra $T^{\ell_1\ell_2}_{\ell_3\ell_4}(\ell)$ and differ in the way they weight various modes, which are specified by a particular choice of the quadruplet $\{\ell_i\}$

$$[T^{(0)}]^{\ell_1\ell_2}_{\ell_3\ell_4}(\ell) = T^{\ell_1\ell_2}_{\ell_3\ell_4}(\ell); \quad [T^{(1)}]^{\ell_1\ell_2}_{\ell_3\ell_4}(\ell) = \frac{1}{4}\left[\Pi_{\ell_1}+\Pi_{\ell_2}+\Pi_{\ell_3}+\Pi_{\ell_4}\right]T^{\ell_1\ell_2}_{\ell_3\ell_4}(\ell); \tag{B10}$$

$$[T^{(2)}]^{\ell_1\ell_2}_{\ell_3\ell_4}(\ell) = \frac{1}{4}\left[\Pi_\ell - (\Pi_{\ell_1}+\Pi_{\ell_2})(\Pi_{\ell_3}+\Pi_{\ell_4})\right]T^{\ell_1\ell_2}_{\ell_3\ell_4}(\ell); \tag{B11}$$

$$[T^{(3)}]^{\ell_1\ell_2}_{\ell_3\ell_4}(\ell) = \frac{1}{4}\left[(\Pi_{\ell_1}+\Pi_{\ell_2}-\Pi_\ell)(\Pi_{\ell_3}+\Pi_{\ell_4}-\Pi_\ell)\right]T^{\ell_1\ell_2}_{\ell_3\ell_4}(\ell). \tag{B12}$$

The four generalized kurtosis and the related kurt-spectra we have defined above can now be expressed in terms of these generalized trispectra $T^{(i)}$ as follows:

$$K^{(i)} = \sum_{\ell_i}\sum_{\ell}[T^{(i)}]^{\ell_1\ell_2}_{\ell_3\ell_4}(\ell)I_{\ell_1\ell_2\ell}I_{\ell_3\ell_4\ell}; \quad K^{(i)}_\ell = \sum_{\ell_i}\frac{1}{\Xi_\ell}[T^{(i)}]^{\ell_1\ell_2}_{\ell_3\ell_4}(\ell)J_{\ell_1\ell_2\ell}J_{\ell_3\ell_4\ell}; \quad K^{(i)} = \sum_\ell \Xi_\ell\, K^{(i)}_\ell. \tag{B13}$$

These kurt-spectra can be estimated using techniques that are very similar to techniques we have employed to estimate the skew-spectra before, e.g. to construct the first of these kurt-spectra we have to cross-correlate the squared field Ψ^2 with itself. Other kurt-spectra are similarly constructed by cross-correlating quadratic constructs which also involve the derivative maps:

$$K_\ell^{(0)} \equiv \frac{1}{\Xi_\ell}\sum_m [\Psi^2]_{\ell m}[\Psi^2]^*_{lm}; \quad K_\ell^{(1)} \equiv \frac{1}{\Xi_\ell}\sum_m [\Psi^2]_{\ell m}[\Psi\nabla^2\Psi]^*_{\ell m}; \tag{B14}$$

$$K_\ell^{(2a)} \equiv \frac{1}{\Xi_\ell}\sum_m [\Psi^2]_{\ell m}[\nabla^2\Psi]^*_{\ell m}; \quad K_\ell^{(2b)} \equiv \frac{1}{\Xi_\ell}\sum_m [\Psi^2]_{lm}[\Psi\nabla^2\Psi]^*_{\ell m}; \quad K_\ell^{(3)} \equiv \frac{1}{\Xi_\ell}\sum_m [|\nabla\Psi|^2]_{\ell m}[|\nabla\Psi|^2]^*_{\ell m}. \tag{B15}$$

We have defined two different estimators $K_\ell^{(2a)}$ and $K_\ell^{(2b)}$ that can be jointly used to construct the kurt-spectra $K_\ell^{(2)}$. The treatment for the masked sky follows exactly the same manner. For individual $K_\ell^{(i)}$, the unbiased estimators can be recovered using exactly the same mode-coupling matrix $\mathbf{M}_{\ell\ell'}$ introduced before in equation (24); we have for the masked kurt-spectra $\hat{K}_\ell^{(i)} = \mathbf{M}^{-1}_{\ell\ell'}\tilde{K}_{\ell'}^{(i)}$. The auto- and the covariance of these estimators can also be estimated using obvious generalization of equation (24) and equation (32), respectively.

The fourth-order expressions for the power spectra associated with MFs $[v_k^{(3)}]_\ell(\nu)$ can be obtained by replacing all one-point $K^{(i)}$s with their two-point counterparts $K_\ell^{(i)}$ in equations (B4)–(B6) (see equation 19 for a similar expression for $[v_k^{(2)}]_\ell(\nu)$ in terms of the generalized skewness parameters). The contributions from the skewness parameters only contribute in the monopole terms. The extraction of the kurt-spectra in the presence of a mask can be carried out analogously to the skew-spectra.

Corresponding cumulant correlators in the real space are given by: $\mathcal{C}^{\Psi^2,\Psi^2}(\theta_{12})$, $\mathcal{C}^{\Psi^2,\Psi\nabla^2\Psi}(\theta_{12})$, $\mathcal{C}^{\nabla\Psi\cdot\nabla\Psi,\Psi\nabla^2\Psi}(\theta_{12})$ and $\mathcal{C}^{\nabla\Psi\cdot\nabla\Psi,\nabla\Psi\cdot\nabla\Psi}(\theta_{12})$. In the limit of zero separation, they collapse to their one-point counterpart, i.e. $\mathcal{C}^{\Psi^2,\Psi^2}(0) = K^{(0)}$, $\mathcal{C}^{\nabla\Psi\cdot\nabla\Psi,\Psi\nabla^2\Psi}(0) = K^{(1)}$, $\mathcal{C}^{\nabla\Psi\cdot\nabla\Psi,\nabla\Psi\cdot\nabla\Psi}(0) = K^{(2)}$ and $\mathcal{C}^{\nabla\Psi\cdot\nabla\Psi,\nabla\Psi\cdot\nabla\Psi}(0) = K^{(3)}$.

On a different note, the power spectra associated with the kurtosis or kurt-spectra are discussed in detail for a scalar field (Munshi et al. 2011a), where two different types of kurt-spectra were introduced in the context of analysis of CMB Temperature maps. These two kurt-spectra $K_\ell^{(2,2)}$ and $K_\ell^{(3,1)}$ both sample the relevant trispectrum. The first of these is constructed from cross-correlating the squared map with itself. The other kurt-spectrum is constructed from cross-correlating a cubic map with the original map. In general, different sets of maps can also be used to form squared and cubic combinations which will probe a mixed trispectra. In the present context, we are interested in the spectra $K_\ell^{(2,2)}$, as the construction of $K_\ell^{(3,1)}$ will involve gradient maps and are more complicated to analyse in a coordinate-independent way. However, such constructions are indeed possible using the spinorial formalism. The physical meaning of these kurt-spectra can be understood more easily in the harmonic domain. As mentioned, each individual mode of the trispectrum is characterized by a specific choice of the set of modes ℓ_i that defines it. These modes each constitute the sides of a quadrilateral whose diagonal is specified by the quantum number ℓ. Note that the kurt-spectra that we have considered here take contributions from all possible configurations of the quadrilateral while keeping its diagonal ℓ fixed.

The estimation of the kurt-spectra from real data is relatively easy, and follows the same methodology as the skew-spectra. The first of these kurt-spectra $K_\ell^{(0)}$ is extracted by cross-correlating the squared field $\Psi^2(\hat{\Omega})$ with itself. The spectrum $K_\ell^{(1)}$ is constructed by cross-correlating $\Psi^2(\hat{\Omega})$ with $\Psi\nabla^2\Psi$. The other two kurt-spectra can likewise be constructed. In each such construction, a scalar map from a product field is generated before it is cross-correlated with another such map.

The corrections to the power spectrum associated with the MFs now can be written in terms of the $K_\ell^{(i)}$, i.e. the kurt-spectra and the various Hermite polynomials as introduced above. The contributions from the lower order statistics such as skewness will only contribute to the monopole term for every MFs. However, the higher multipoles will involve contributions from various kurt-spectra as indicated in equations (B4)–(B6). Different specific choice of trispectra will therefore lead us to completely different power spectra associated with the MFs and can help to distinguish various models of NG.

The generalized skew- and kurt-spectra can also be useful in probing the detection of topological defects through their effect on change in topology of the CMB temperature (Regan & Shellard 2010).

APPENDIX C: 3*j* SYMBOLS

We list here various expressions related to 3*j* symbols (Edmonds 1968) that were used in the text

$$\begin{pmatrix} \ell_2 & \ell_1 & \ell_3 \\ m_2 & m_1 & m_3 \end{pmatrix} = (-1)^{\ell_1+\ell_2+\ell_3}\begin{pmatrix} \ell_1 & \ell_2 & \ell_3 \\ m_1 & m_2 & m_3 \end{pmatrix} \tag{C1}$$

$$\sum_{\ell_3 m_3}(2\ell_3+1)\begin{pmatrix} \ell_1 & \ell_2 & \ell_3 \\ m_1 & m_2 & m_3 \end{pmatrix}\begin{pmatrix} \ell_1 & \ell_2 & \ell \\ m_1' & m_2' & m \end{pmatrix} = \delta_{m_1 m_1'}\delta_{m_2 m_2'} \tag{C2}$$

$$\sum_{m_1 m_2}\begin{pmatrix} \ell_1 & \ell_2 & \ell_3 \\ m_1 & m_2 & m_3 \end{pmatrix}\begin{pmatrix} \ell_1 & \ell_2 & \ell_3' \\ m_1 & m_2 & m_3' \end{pmatrix} = \frac{\delta_{\ell_3 l_3'}\delta_{m_3 m_3'}}{2\ell_3+1} \tag{C3}$$

$$(-1)^m \begin{pmatrix} \ell & \ell & \ell' \\ m & -m & 0 \end{pmatrix} = \frac{(-1)^\ell}{\sqrt{(2\ell+1)}} \delta_{\ell' 0}. \tag{C4}$$

The Gaunt (or overlap) integral involving three spherical harmonics can be expressed in terms of $3j$ symbols:

$$\int \mathrm{d}\hat{\Omega}\, Y_{\ell_1 m_1}(\hat{\Omega}) Y_{\ell_2 m_2}(\hat{\Omega}) Y_{\ell_3 m_3}(\hat{\Omega}) = \sqrt{\frac{(2\ell_1+1)(2\ell_2+1)(2\ell_3+1)}{4\pi}} \begin{pmatrix} \ell_1 & \ell_2 & \ell_3 \\ 0 & 0 & 0 \end{pmatrix} \begin{pmatrix} \ell_1 & \ell_2 & \ell_3 \\ m_1 & m_2 & m_3 \end{pmatrix}. \tag{C5}$$

This paper has been typeset from a TEX/LATEX file prepared by the author.